Journal of Volcanology and Geothermal Research 182 (2009) 182–200

Contents lists available at ScienceDirect

Journal of Volcanology and Geothermal Research

journal homepage: www.elsevier.com/locate/jvolgeores

Deformation of Stromboli Volcano (Italy) during the 2007 eruption revealed by radar interferometry, numerical modelling and structural geological field data

Nicola Casagli [a,*], Alessandro Tibaldi [b], Andrea Merri [c], Chiara Del Ventisette [a], Tiziana Apuani [c], Letizia Guerri [a], Joaquim Fortuny-Guasch [d], Dario Tarchi [d]

[a] Department of Earth Sciences, University of Firenze, V. la Pira 4, 50121 Firenze, Italy
[b] Department of Geological Science and Geotechnologies, University of Milan-Bicocca, P. della Scienza 4, Milan, Italy
[c] Department of Earth Sciences "Ardito Desio", University of Milan, Via Mangiagalli, 34, 20133 Milano, Italy
[d] Joint Research Centre, Institute for the Protection and Security of the Citizen - IPSC, European Commission, V. E. Fermi 1, 21020 Ispra (VA), Italy

ARTICLE INFO

Article history:
Received 1 April 2008
Accepted 3 January 2009
Available online 16 January 2009

Keywords:
Stromboli volcano
monitoring
radar interferometry
numerical modelling

ABSTRACT

The activity of Stromboli volcano is characterized by very low energy explosions, occurring every 10–15 min, throwing out lava above the crater rim. During 2007, the volcano showed an anomalous activity in which new effusive vents developed (27 February and 9 March) and a major explosion took place on 15 March. This paper presents an integrated study based on a structural geological field survey, interferometric radar monitoring and numerical modelling on the deformations of the upper NW flank of the volcano (Sciara del Fuoco — SdF). The field survey carried out during the 2007 events shows the development of mainly NE-striking fissures and fractures on the northern part of the upper SdF. In January 2007, the ground-based synthetic aperture radar (GB-InSAR), installed on the flank of the SdF, showed a progressive acceleration of movement on the NE crater preceding the eruption of 27 February 2007. By the first half of February, the acceleration also involved the upper portion of the SdF and on 27 February the eruption started with the opening of new vents and deformation rates higher than the measurement capability of the radar device. On 8–9 March 2007, the GB-InSAR highlighted the formation of a bulge on the NW sector of the SdF, preceding the opening of an additional vent. To understand the deformation pattern recorded during the eruption, a numerical simulation was carried out by using the FLAC 3D code. Based on the integration of all the data, the deformations observed in the pre-effusive phase (before 27 February) seem to be related to the intrusion of a SW–NE striking dyke. The bulging recorded before the 9 March vent opening is instead to be associated with the intrusion of a sub-horizontal sill.

1. Introduction

Stromboli Island represents the 976-m-high emerged portion of a volcanic cone located in the Tyrrhenian Sea 60 km North of Sicily (Italy). The island rises from a depth of about 2500 m below sea level. One of the most evident geomorphological features is a major depression, known as Sciara del Fuoco (SdF), which has developed on the NW side of the volcano following a series of lateral collapses mainly during the Holocene (Tibaldi, 2001). The activity of Stromboli is characterized by very low energy explosions (Strombolian activity) occurring at intervals of about 10–15 min from the vents located on the summit crater area. The normal strombolian activity is periodically interrupted by more energetic explosions (1–2 per year) and by sporadic effusive episodes characterized by the effusion of shoshonitic basalts (every 10–20 years). The eruptive vents are mainly located in the NE sector of the Sciara del Fuoco depression and, generally, each effusive episode produces a volume of lava of about 100 m^3.

In February 2007, the Stromboli activity quickly changed and, on 27 February, a new effusive phase occurred. During this "anomalous" activity, effusive vents developed at an elevation of 600 m a.s.l. and 400 m a.s.l. On 9 March, another vent opened at an elevation of 500 m a.s.l. while a major explosion occurred on 15 March. This phase of activity lasted until 12 April 2007.

This paper presents an integrated study of the 2007 Stromboli eruption and of the related deformations. The study is based on structural geological surveys, interferometric radar monitoring and numerical modelling of the effects of propagating sheet intrusions on the deformation field of the NW volcano flank. The data collected during the structural geological survey after the 2007 eruption are compared with the pre-existing structural setting. These data, associated with the interferometric radar monitoring, allow an accurate reconstruction of the induced ground deformations and an evaluation of the tensional field of the volcano.

Furthermore, this paper aims at understanding the possible presence of the effusive and explosive precursors and confirms the importance of a multi-disciplinary approach to forecast a tensional crisis of the system by considering the deformation pattern before an

* Corresponding author. Tel.: +39 055 2757523; fax: +39 055 2756296.
E-mail address: nicola.casagli@unifi.it (N. Casagli).

0377-0273/$ – see front matter © 2009 Elsevier B.V. All rights reserved.
doi:10.1016/j.jvolgeores.2009.01.002

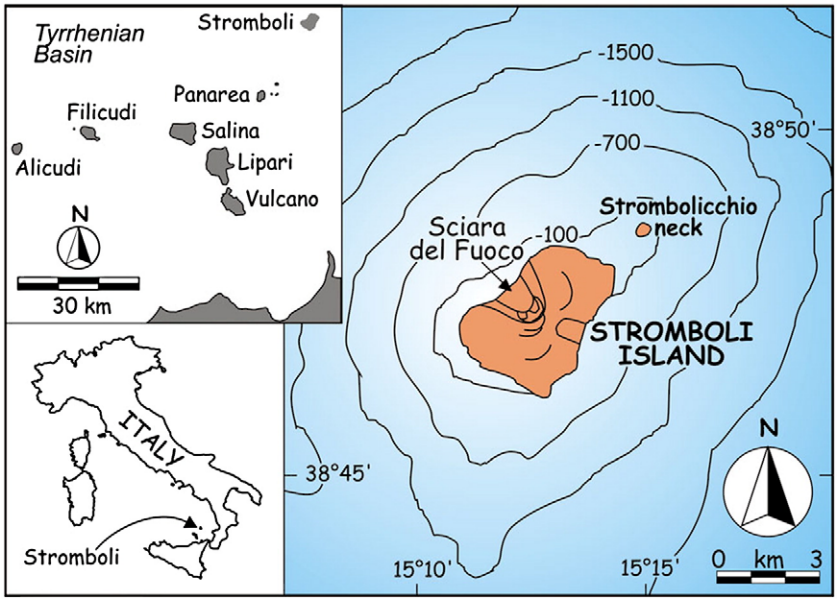

Fig. 1. Location of Stromboli volcano within the Aeolian Archipelago.

eruption. Indeed, the magma intrusion occurring before the effusion induced deformations on the SdF and on the crater flank that were assessed by the radar apparatus.

The scenarios of the deformation of active volcanoes can be quite complex, because they can result from the resultant of gravity, magmatic and tectonic forces, which may act at the same time (i.e. Voight and Elsworth, 1997; Voight, 2000; Sachpazi et al., 2002; Tibaldi et al., 2008a). Moreover, different intrusion geometries can produce various deformation patterns at the surface (i.e. Muller and Pollard, 1977; Delaney et al., 1986; Pollard and Segall, 1987; Gudmundsson and Loetveitz, 2005) that in turn can be enhanced, or even distorted, by gravity sliding. As it appears from the data presented here, in such complex situations only a synthesis of different methodologies can provide the most reliable results for interpreting the magma paths rising to the surface. The combination of geophysical radar data with structural geological field data and numerical modelling, proposed in this paper, provide a useful tool for the interpretation of the signals of active volcanoes.

2. Geological background

The island of Stromboli belongs to a large volcanic complex, located at the NE tip of the Aeolian archipelago, consisting of two main centres: Stromboli and Strombolicchio (Fig. 1). Available off-shore data indicates that it rises 2.6 km from the sea floor (Gabbianelli et al., 1993; Romagnoli et al., 1993). The Stromboli volcano dates back to 100 ky BP to the present (Gillot and Keller, 1993).

The Stromboli feeding system is revealed by a complex sheet pattern. Sheets and fractures are not arranged in a typical radial pattern as observed in the summit zone of other composite volcanoes (Chevallier and Verwoerd, 1988; Manetti et al., 1989; Ferrari et al., 1993), but they have preferentially developed along a NE-trending rectilinear axial zone (Tibaldi, 1996, 2001). Sheet arrangement is complicated by a N–S zone of injection in the southern flank of the volcano, and by an E–W and a WNW–ESE trending zones in the western flank (Corazzato, 2005; Corazzato et al., 2008). The present activity occurs through a series of vents nested into the active composite crater; these vents are mostly aligned NE–SW reflecting the presence of a NE-striking active dyke (Tibaldi, 1996; Chouet et al., 2003; Tibaldi, 2003).

The structure of the Stromboli volcano is complex, because of its alternating building and destructive phases. A series of coaxial escarpments testify the long history of its instability, although some of the escarpments resulted from vertical caldera-type collapses, whereas others were produced by lateral major failures.

The oldest collapse of the island (Unit 1 in Fig. 2) was interpreted as a caldera by Pasquarè et al. (1993) and occurred during the interval 64–85 ky BP. This was followed by the deposition of a series of rock units (Fig. 2) alternated by other caldera collapses and one lateral collapse towards the SE (Tibaldi et al., 1994; Tibaldi, 2001; Tibaldi, in press).

The most recent Neostromboli (NS) deposits (Keller et al., 1993) partially cover a large area of the NW side of the volcano onlapping and hiding a depression escarpment cut into the Upper Vancori (UV) deposits (Unit 5 in Fig. 2). This horseshoe-shaped rim represents the remnant of the earliest large sector collapse dated 13 ky BP. The Neostromboli deposits terminate against an escarpment formed during another sector collapse (Unit 6 in Fig. 2) dating back to the Holocene. The most recent unit, proposed by Keller et al. (1993) and named Recent Stromboli (RS), is mainly confined to the NW of the UV rim. It has recently been subdivided into a series of units interleaved by two further collapse structures (Tibaldi, 2001, in press; Fig. 2). This RS succession indeed shows several unconformities pointing to the onlap on the escarpments of UV (Unit5), of NS (Unit 6), and of other flank collapse deposits (Unit 7 in Fig. 2), which affected the Pizzo Sopra la Fossa pyroclastic cone. Successively, the last flank collapses (Unit 8 in Fig. 2) occurred, ending in the formation of the present depression known as Sciara del Fuoco (SdF). In the last 1–2 ky, this depression has been only partially filled by thin lava flows and the active pyroclastic cone in the upper part of the scar. Other Holocene products erupted along NE-trending fissures or vents that are mainly located in the NE part of the island (Fig. 2).

3. Field structural geological data

The main structural observations carried out in the field during the 2007 events at the summit of the volcano, are summarized in this section, together with some data collected during previous years.

The area affected by the events of February–April 2007 belongs to the northern sector of the SdF. This area corresponds exactly to the zone affected by fissuring, lava emission and landsliding during the previous eruption of 2002–2003. It is also important to reconstruct the general framework of the deformation of the entire SdF. Based on field data, in fact, it emerges that since 2000 a series of fissures started

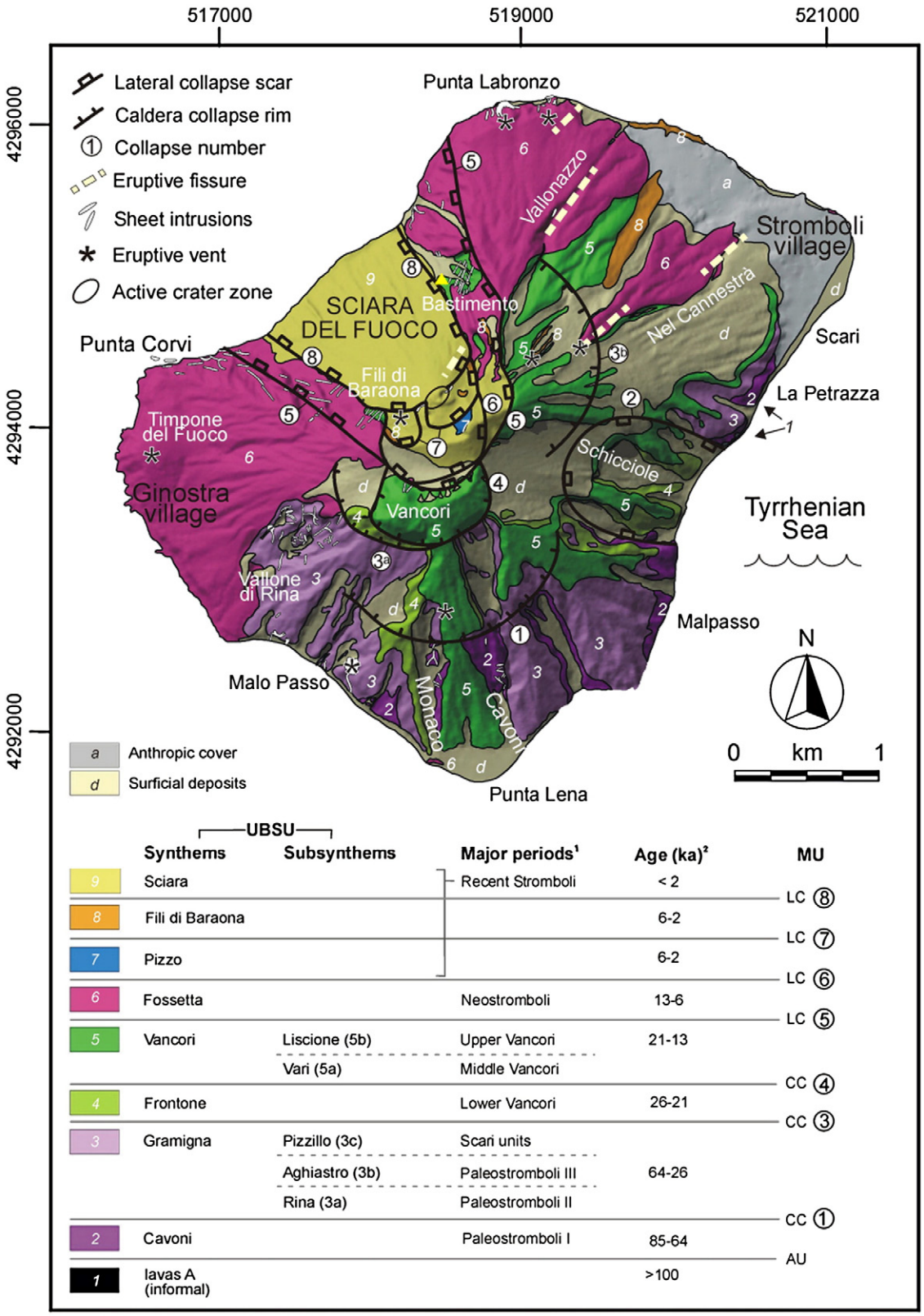

	Synthems	Subsynthems	Major periods[1]	Age (ka)[2]	MU
9	Sciara		Recent Stromboli	< 2	
8	Fili di Baraona			6-2	LC ⑧
7	Pizzo			6-2	LC ⑦
6	Fossetta		Neostromboli	13-6	LC ⑥
5	Vancori	Liscione (5b)	Upper Vancori	21-13	LC ⑤
		Vari (5a)	Middle Vancori		
4	Frontone		Lower Vancori	26-21	CC ④
3	Gramigna	Pizzillo (3c)	Scari units		CC ③
		Aghiastro (3b)	Paleostromboli III	64-26	
		Rina (3a)	Paleostromboli II		
2	Cavoni		Paleostromboli I	85-64	CC ①
1	lavas A (informal)			>100	AU

UBSU

Fig. 2. Map of the Stromboli Island, originally at a 1:50 000 scale, obtained after reduction from the map at a 1:10 000 scale of Tibaldi (in press). The legend provides the names of the synthems, their age, and a correlation with the units previously established in the map by Keller et al. (1993). A very important characteristic of Stromboli is that the activity of cone growth has been repeatedly interrupted by collapses, both of summit caldera (i.e. vertical collapse) and of lateral collapse type. The symbols used here enable these types to be distinguished. UTM coordinates are in meters. The yellow triangle on the flank of the Sciara del Fuoco represents the GB-InSAR.

to develop along the southern part of SdF (Fig. 3). These fissures were not present during autumn 1999 and were first observed during May 2000 (Tibaldi et al., 2003). Three main fissures, striking NE–SW, formed along the upper part of the southern sector of the SdF and propagated towards the active crater zone. Due to the high risk induced by the volcanic activity and rolling stones it was not possible

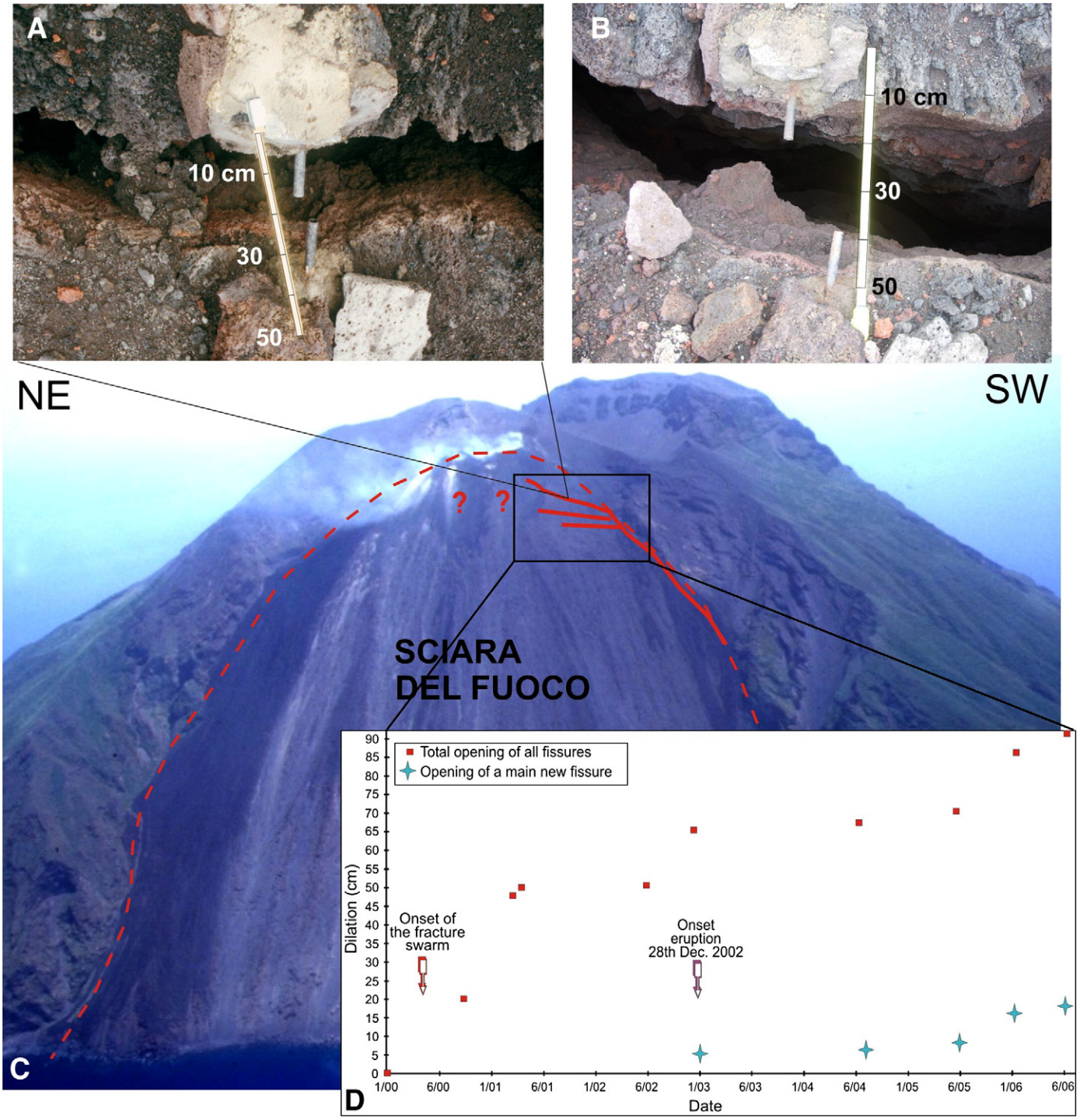

Fig. 3. Fissures opened in 2000 and their 2000–2006 measurements. A. Photo of one of the NE-striking fissures (the two lines converge to the point where the photo has been taken) with two cemented steel piercing points, offset portrayed in September 2000. B. Photo of the same fissures of A, offset in January 2006. C. Photo of the Sciara del Fuoco with the boundary of the last lateral collapse from the late Holocene (dashed line) and trace of the main fissures developed since 2000. Their possible extension NE (question points) was never checked in the field due to the high risk near the active crater zone. D. Graph resuming some of the measurements taken along the fissures from 2000 to 2006.

to carry out the field survey on their possible prolongation towards the NE. Similarly, it was impossible to check if this fissures swarm was also present on the opposite side of the crater, i.e. in correspondence with the area of the 2002–2003 and 2007 eruption. However, the total dilation measured along these fissures did not decrease towards the NE. This suggests that the zone of disappearing of the surface trace of these fissures might not be the real structural termination of the covering effect produced by the continuous debris and pyroclastic ejecta thrown out from the crater. Towards the south, these three main fissures were linked with a main left-lateral slip plane striking parallel to the southern flank of the SdF depression. In the following years, the fissures increased in number and in offset (Fig. 3D). The total cumulative component of pure dilation was measured at intervals of 6 months by direct field inspections; in 2000 a series of stainless still tubes were fixed through concrete across the fissures. After complete concrete hardening, the tubes were cut in the middle in order to use their ends as piercing points for measuring offset increases. Three-dimensional measurements were made with a laser of a 1 mm

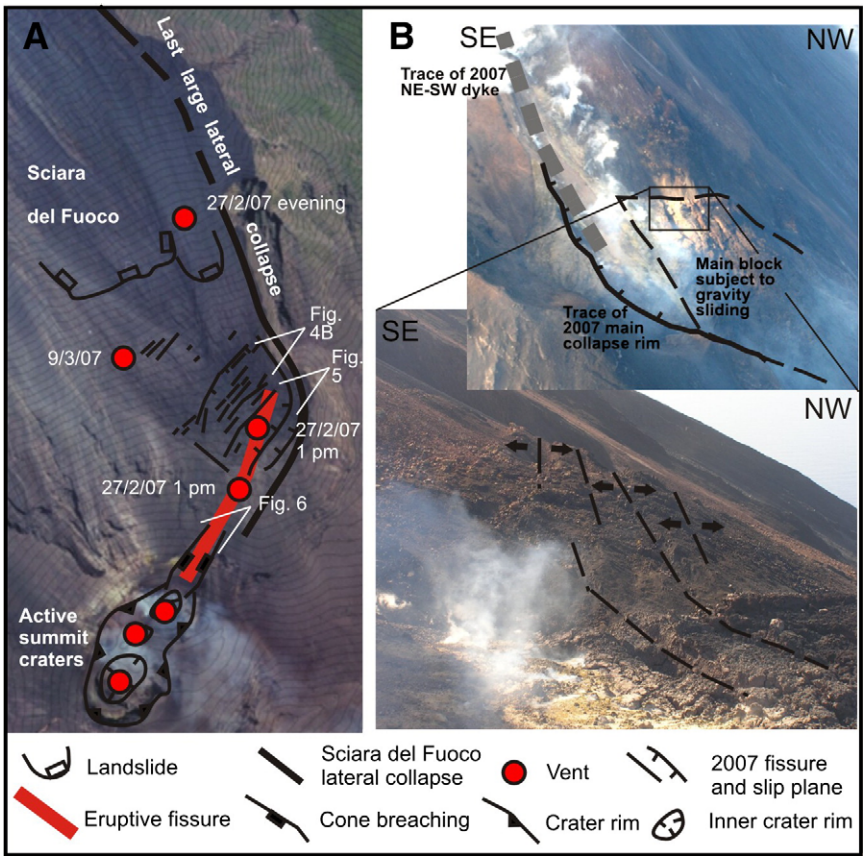

Fig. 4. A. Main volcano-tectonic structures of the northern part of Sciara del Fuoco. The three summit vents have been historically active, whereas the other four vents opened during the eruption of 2007. The open angles indicate the view of the photographs. B. Upper photo: general view from a helicopter of the summit affected by the February–April 2007 events. The dashed grey line represents the surface trace of the NE-striking dyke which propagated through the N flank of the summit pyroclastic cone. The scarp rim is the same as Fig. 5. The dashed black line encircles the main zone of seaward collapse. Lower photo: a closer look at the structures affecting the upper part of the zone of collapse. Note the presence of a series of metre-wide fissures, locally passing through slip planes, striking NE–SW. Arrows indicate the average direction of dilation. For view direction see (A).

resolution. The cumulative offset reached 1 m in 6 years, whereas a component of dip-slip appeared after about one year, totalling some decimetres in 6 years, with a downthrown mostly occurring on the seaward blocks. It is interesting to note that an increase in the total offset along these structures was observed just before the 2002–2003 eruption after a period of more than 1 year (from March 2001 to June 2002) without significant deformation. During the onset of the 2002–2003 crisis (28 December 2002) another fissure appeared, followed by quite a constant offset increase (Fig. 3D).

On the opposite northern part of SdF, a series of NE-striking lineaments were observed during the 2001–2002 period, although it is not possible to have precise field data on their kinematics. This zone was also completely disrupted by the 2002–2003 eruption. The lava field emplaced during the 2003 effusions was in turn affected by a series of fractures and fissures with two main orientations: NW–SE, i.e. parallel to the local orientation of the SdF flank. At the beginning of the 2007 eruption the summit area of the northern part of SdF was affected by a series of morphostructural changes with precise and constant geometries. The first data observed at the onset of the eruption (27 February 2007, 12:30 UT) were obtained by a thermal camera located at the summit of the volcano and looking southwards (Calvari et al., 2009-submitted for publication). The camera clearly detected a positive thermal gradient developing across the NE flank of the summit active pyroclastic cone. This thermal feature has a rectilinear geometry with a NE–SW strike. It was followed, after a few seconds, by the appearance of another positive thermal gradient further to the NE, at the foot of this pyroclastic cone. Helicopter and field surveys in the following days indicated that on 27 February 2007 a breaching of the NE summit pyroclastic cone flank occurred and that a new lava emission took place from a NE-striking fissure, located at an altitude of about 600 m a.s.l. at the foothill of the northern pyroclastic cone (Fig. 4A). The breaching of the pyroclastic cone flank is V-shaped in section with two almost parallel to sub-parallel flanks, mostly striking NE–SW. It is believed that all these features, based both on thermal data and field surveys, indicate the presence of a NE–SW striking dyke that propagated across the NE flank of the summit pyroclastic cone (Fig. 4). On the evening of the same day, a new vent opened at approximately 400 m a.s.l. (Fig. 4A).

In the days following the 27 February, a series of fractures mostly striking NE–SW developed in the lava field expanding in the upper part of the northern SdF, around 600 m a.s.l. These fractures turned into fissures and slip planes (Fig. 4A). The slip planes with the highest offset appeared in upper part of the lava field, giving rise to a series of steps with northwest facing scarps and a downthrow of the seaward blocks (Fig. 5). In correspondence to the initial 27–28 February lava vents, a series of NE striking fractures and fissures showed degassing at high temperature, also suggesting the presence of a NE trending magmatic feature (Fig. 5). Further to the NW along the northern SdF, a huge area showed diffuse NE striking structures (Fig. 4B). These structures locally show a dip-slip component of motion. The direction of dilation, as measured normally to the average fissure strike, indicates a dominant NW–SE direction of extension.

These deformative events caused a series of new outcrops, one of which gives clues to the inner structure of the northern part of the summit pyroclastic cone (Fig. 6). This is affected by a series of slip planes dipping towards the NW, i.e. towards the sea, at angles of 60–80°. Field observations indicate the presence of normal offsets with a downthrow of the seaward blocks. It is important to note that, due to their steep inclination, these planes should not be directly linked with

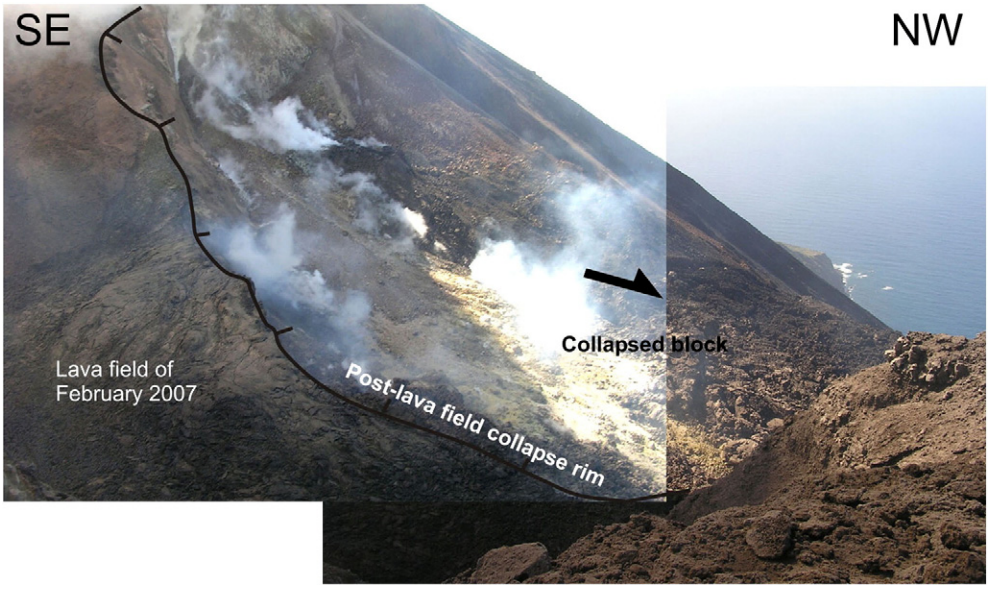

Fig. 5. General view of the summit affected by the February 2007 lava effusion. During the first phase a lava plateau formed at the foot of the N active vent zone. Successively, the seaward part of this lava plateau collapsed producing the scarp rim evidenced here. For view direction see Fig. 4A.

surface landsliding; instead they could represent planes of weakness related to deep deformations of the SdF.

4. Radar interferometry

4.1. GB-InSAR technique

The Synthetic Aperture Radar (SAR) interferometry (Curlander and McDonough, 1991) has become, in recent years, one of the emerging techniques for the measurement of ground displacements and an operational tool for monitoring and early warning. The ground-based SAR interferometry (GB-InSAR; Tarchi et al., 1997; Rudolf et al., 1999; Tarchi et al., 2000; Atzeni et al., 2001; Tarchi et al., 2003; Antonello et al., 2004a) provides displacement measurements over areas of up to a few square kilometres with sub-millimetre precision and high temporal frequency of acquisition (revisiting time of a few minutes). After the Stromboli eruption of December 2002, the National Civil Protection Department (DPC) and the National Institute for Geophysics and Volcanology (INGV) set up an extensive monitoring system on the Stromboli volcano; the Earth Sciences Department of the University of Florence, was involved by the DPC for installing a GB-InSAR apparatus for real-time monitoring of ground deformations on the flank of the SdF.

The GB-InSAR system installed on the Stromboli Island was designed by the Joint Research Centre of the European Commission (Rudolf and Tarchi, 1999). The system consists of a ground-based interferometer, known as LISA (Linear SAR). The apparatus was installed at an elevation of 400 m a.s.l. on a stable zone of the northern flank of the SdF, at an average distance from the target area of about 600 m, pointing upwards to the NE crater. The GB-InSAR apparatus has been continuously active in Stromboli since 20 February 2003 (Antonello et al., 2003; Casagli et al., 2004; Antonello et al., 2007) and produces, on average, 120 images per day of the area under investigation. The hardware consists of a continuous-wave step-frequency (CW-SF, central frequency of 17.05 GHz) radar that realizes a synthetic aperture by moving antennas along a horizontal straight rail that is 3 m long.

As radar images (produced every 12 min) are obtained through sampling techniques, frequency and spatial steps have to be selected in order to avoid ambiguity in range and cross-range. Range and cross-range resolution (about 2 m × 2 m, with a precision of measurement of less than 1 mm) in the radar image are related respectively to the

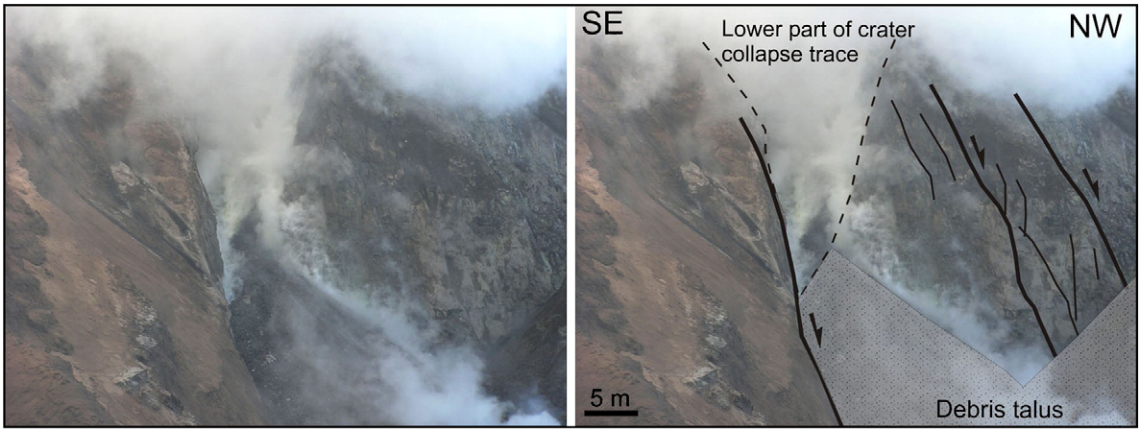

Fig. 6. Main structures cropping out in the zone at the foot of the N vent, where the 2007 eruption occurred, 8 March 2007. Photo taken looking S (on the left) and the interpretation (on the right). Note the presence of a series of steep slip planes dipping toward NW, i.e. towards the sea. For view direction see Fig. 4A.

swept bandwidth and to the overall scan length. The observed area covers the NW flank of the crater and the upper part of the SdF. Synthesized radar images can be projected on the digital elevation model (DEM) of the test site as shown in Fig. 7.

Interferograms are obtained using pairs of averaged sequential images. The interferogram does not contain topographic information, since the position of the antennas remains the same during different scans (zero baseline condition). Through the phase difference of the backscattered signal in different times, it is possible to estimate the displacement, considering that a complete interferometric fringe corresponds to 8.8 mm (in this configuration). It is possible to assess only the component of the displacement vector along the line-of-sight (LoS) in the time interval between two acquisitions. The LoS vector represents the line joining the radar to each point of the observed scenario so that each pixel of the radar image has a different LoS. Negative values of displacement indicate a movement towards the sensor (shortening along the LoS). On the crater area this direction of movement corresponds to the inflation of the volcanic cone, while on the SdF this is usually related to a local bulging or to the downslope sliding of the volcano-clastic material accumulated on the SdF slope. Conversely, a positive value of displacement identifies a movement backwards with respect to the sensor (lengthening along the LoS) that, on the crater area, could be related to the deflation of the volcanic cone. Deformation maps are obtained by cumulating the displacements measured by interferograms derived from each couple of consecutive images. Because of the short time interval (12 min)

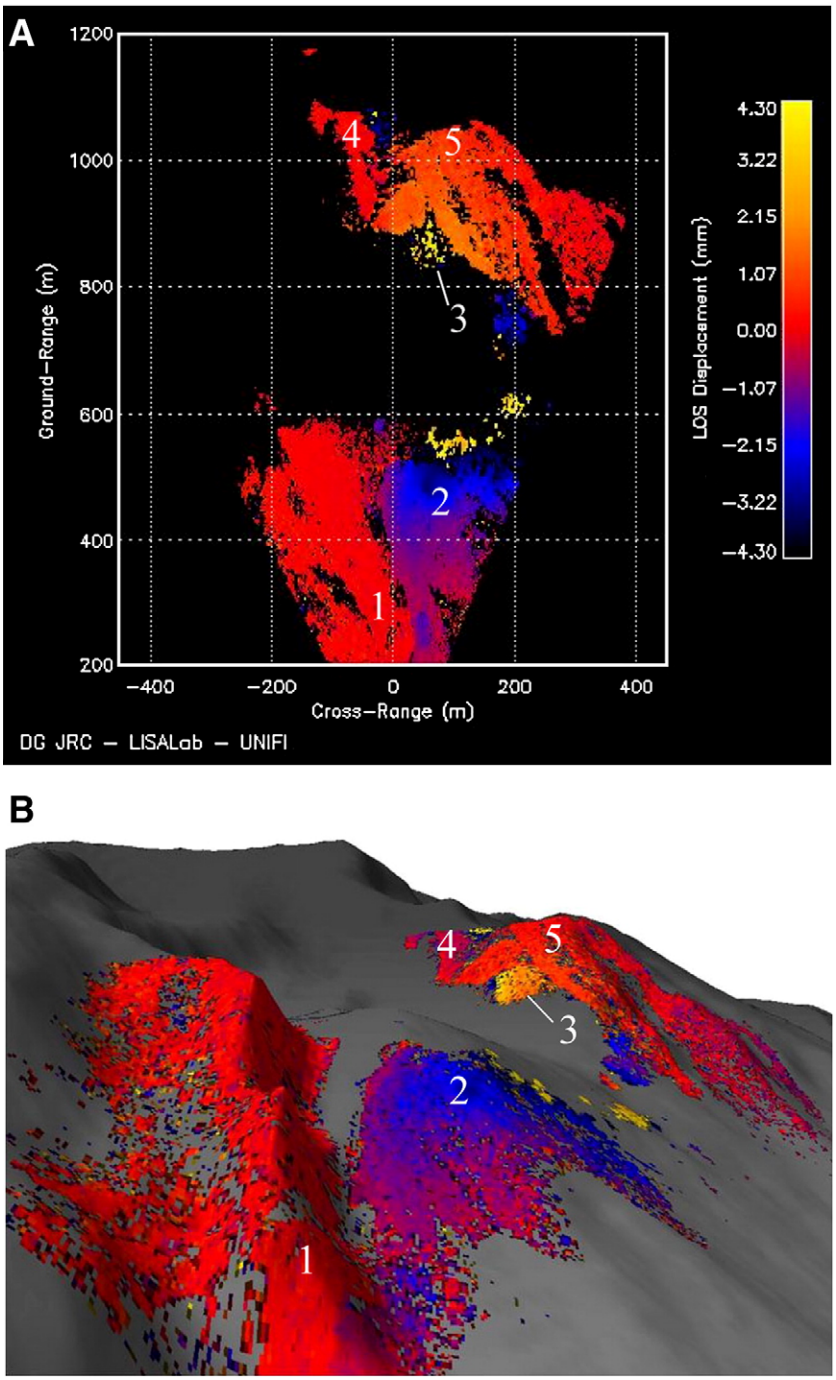

Fig. 7. (A) Interferogram between 19:38 UT and 21:35 UT of 8 March (time interval of 1 h and 58 min) (B) Interferogram projected on DEM with the main sectors of the target area: 1) The "Bastimento" stable area; 2) Sciara del Fuoco upper sector; 3) pyroclastic cone; 4–5) NE crater sectors.

between two consecutive scans, these interferometric displacements are usually smaller than half-wavelength, so unwrapping procedures are not necessary.

4.2. Deformations during the 2007 eruption from GB-InSAR

In the first months of 2007, the GB-InSAR data allowed the identification of three different phases: (1) the pre-effusive phase (from 10 January to 27 February; green area in Fig. 8), characterized by very low, progressively increasing, deformation rates; (2) the effusive phase (from 27 February to 12 April; magenta area in Fig. 8) characterized by very high velocity of deformation and (3) the post-effusive phase (from 12 April; yellow area in Fig. 8), in which the deformation rates decreased down to the pre-eruption values. Velocity values are plotted in Fig. 8 in absolute value: the red line represents movements towards the sensor (negative radar displacements), while the blue line represents movement backwards with respect to the sensor (positive radar displacements).

During the pre-effusion phase (phase 1), starting from 10 January, the GB-InSAR data allowed the identification of a continuous acceleration on the crater area. Indeed, the recorded velocity progressed from 0.04 mm/h to 0.7 mm/h towards the radar. The interferometric fringes, developed from January on the crater flank, shows a concentric pattern around the crater (Fig. 9), thus suggesting a radial deformation. This is consistent with the inflation of the upper sector of the volcanic system.

The increase in the deformation rate was initially clearly visible only on the upper part of the volcano (crateric sector), and successively involved the other sectors of the monitored area down the SdF (15 February; Fig. 9). Since 15 February, the GB-InSAR recorded, on the upper part of the SdF, a sudden increase in velocity from 0.02 mm/h to 0.25 mm/h towards the sensor, which was maintained until the eruption of 27 February.

In this period the interferograms show a deformation pattern mainly localized on the NW upper sector of the SdF. The interpretation of this localized deformation is an effect of the bulging related to the

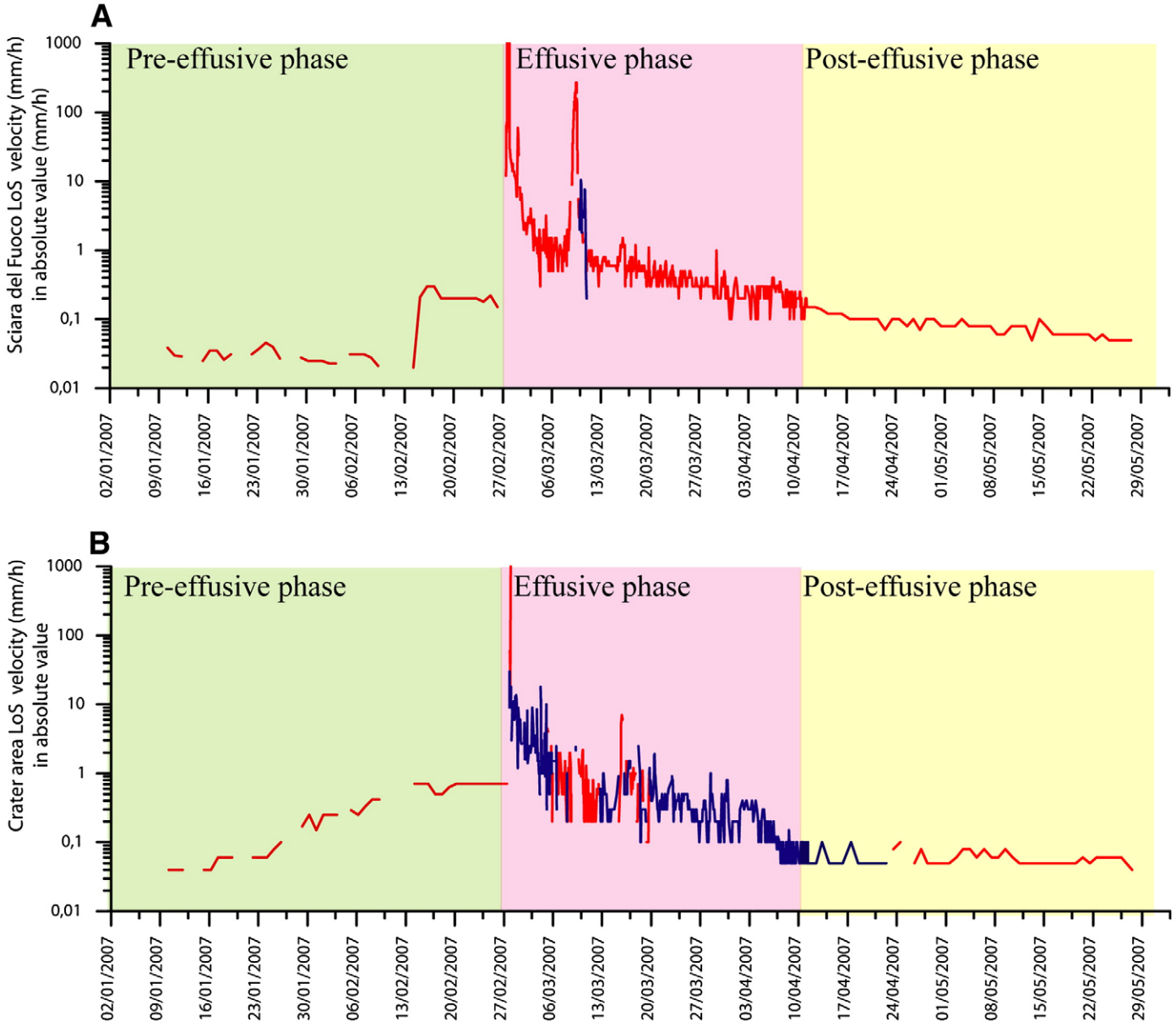

Fig. 8. GB-InSAR velocity during the 2007 Stromboli eruption measured on the Sciara del Fuoco (A) and on the crater (B) sectors. LoS velocity is in logarithmic scale to emphasize the low displacement rate in the first period of the pre-effusion phase and in the post-effusion phase. The red line represents a displacement toward the SAR sensor (negative radar displacement); the blue line represents the deformation back to the SAR sensor (positive radar displacement).

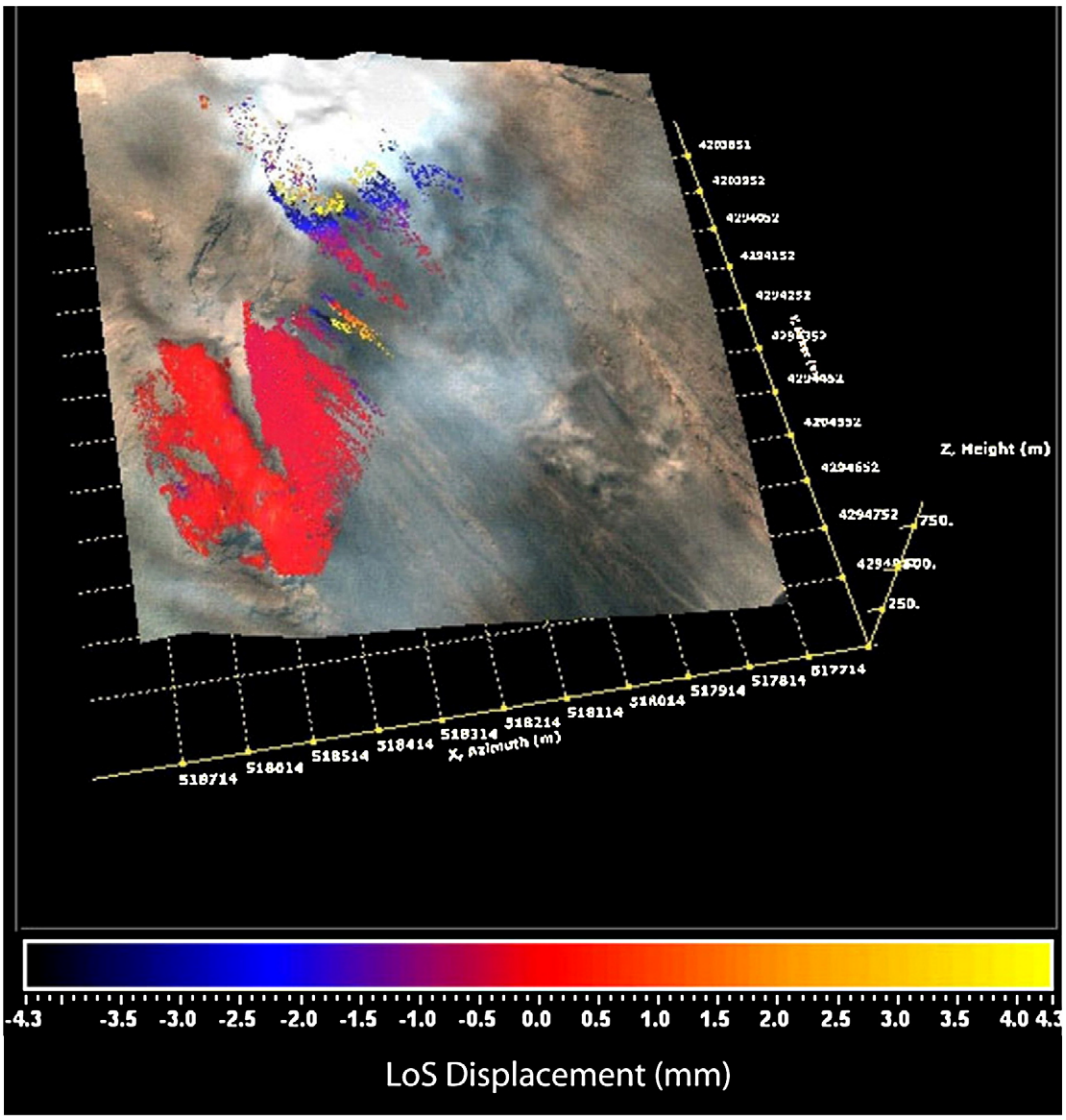

Fig. 9. Interferogram projected on orthophoto draped on DEM, between 08:11 UT of 15 February and 05:37 UT of 16 February (time interval of 21 h and 26 min), showing pre-effusive deformations on the crateric zone and on the upper sector of the SdF.

development of the new effusive vent at 600 m a.s.l., occurred at 13:02 UT of 27 February. This is particularly evident on the interferogram shown in Fig. 10, which spans a time interval of 22 min from 12:43 UT to 13:05 UT on the same day.

The effusive phase (phase 2; from 27 February to 12 April), starts with an explosion occurred at 12:30 UT, with the consequent collapse of a portion of the crater flank, occurred at 12:48 UT, and with the opening of an effusive vent at 600 m a.s.l., occurred at 13:02 UT. The interferogram in Fig. 10 shows a complete decorrelation on the crater due to the explosion and to morphological changes related to the crater collapse; it also shows the interferometric fringes on the SdF due to the bulging related to the vent opening at 600 m a.s.l.. The opening of a second vent at 400 m a.s.l., occurred in the afternoon, was not observed by the GB-InSAR, since that sector of the SdF is out of the field of view of the instrument and since the SdF was completely decorrelated from 14:41 UT to 19:08 UT.

The last coherent interferograms (between 13:38 UT and 14:41 UT, i.e. Fig. 11) before the general decorrelation indicates that a new deformation pattern was established on the SdF, which is strictly related to landslide movements. Indeed, the interferometric fringes are roughly perpendicular to the slope dip direction.

The long period of decorrelation above mentioned, is due to the high values of velocity related both to the effusive activity and to the landslides associated to the collapse of the upper part of the SdF, occurred at 18:30 UT.

Since 19:08 UT, coherence was re-established on the SdF and interferograms showed a deformation pattern resulting from the combination of two distinct factors: a) the first one concerns only the area near the NE flank (the so-called Bastimento area; sector 1 in Fig. 7) and the central part of the slope, in which irregular deformations were caused by lava flows; b) the second one, involving the whole slope of SdF, is related to the gravitational sliding of the slope at an average rate of 15 mm/h, locally disturbed by irregular and high speed deformations, related to shallow landslides and other slope movements.

During the entire effusive phase, these velocity values, on the SdF, showed a constant decrease from 30 mm/h to 0.2 mm/h towards the sensor, with the only exception of two limited periods, related to the opening of the 500 m a.s.l. vent (on 8–9 March) and to the major explosion (on 15 March).

Since 8 March the velocity recorded on the SdF increased again, with movements towards the sensor (Fig. 8). The interferometric fringes showed a concentric arrangement around the NW zone of the upper SdF (about the same zone on which high deformations were

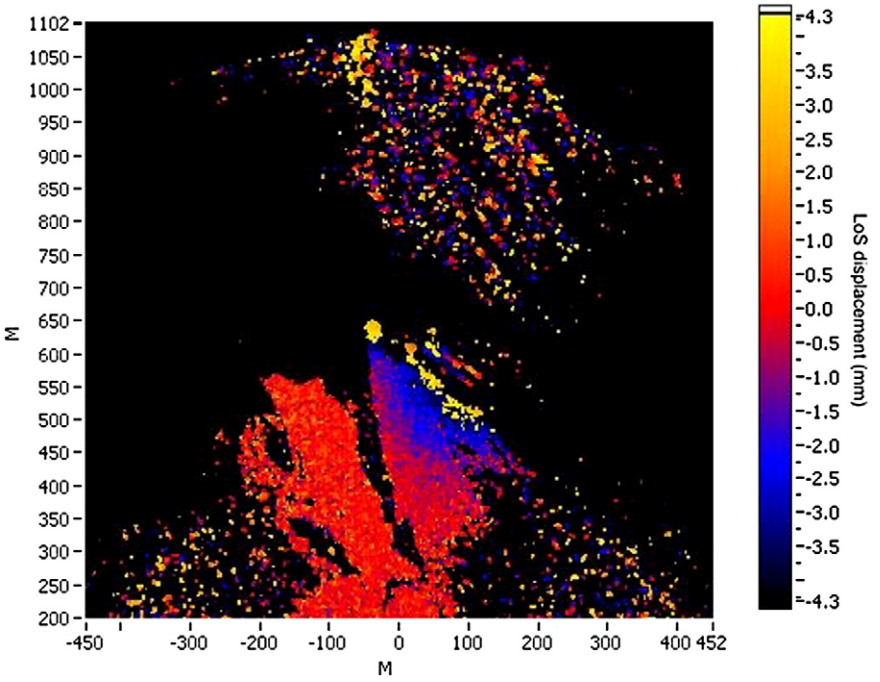

Fig. 10. Interferogram between 12:43 UT and 13:05 UT of 27 February (time interval of 22 min), showing a complete decorrelation on the crater flank caused by the explosion that occurred at 12:30 UT. A clear pattern of interferometric fringes on the NW part of the SdF are shown related to a bulging deformation due to the vent opening at 600 m a.s.l. occurred at 13:02 UT.

recorded since 15 February). The interferogram with a time interval of 11 min (from 11:17 and 11:28 UT of the 9 March 2007; Fig. 12) highlights a very high deformation rate (more than 300 mm/h), which again exceeds the capability of the correct phase unwrapping. The wider red areas in Fig. 12 are stable; each colour sequence red–blue–yellow–red represents an interferometric fringe corresponding to a displacement of 8.8 mm. According to our interpretation, the arrangement of these interferometric fringes is related to the bulging caused by the opening of a new vent. Indeed, at the 14:30 UT of 9 March, the new effusive vent opened at 500 m a.s.l. In order to defining a warning model for assessing the onset time of the tensional crisis related to the opening of the vent, the inverse velocity was plotted against time (Fig. 13), following the method proposed by Fukuzono (1985a,b, 1990) and Voight (1988, 1989). From Fig. 13 it is clear that the opening of the 9 March vent can be predicted in advance of one day. Considering the linear trend of the last records, the "time of failure" was actually predicted at 14:00 UT of 9 March and the warning was sent to the Civil Protection authorities.

The last major event of the effusive phase was the explosion on 15 March. The velocities on the SdF sector, recorded between the opening of

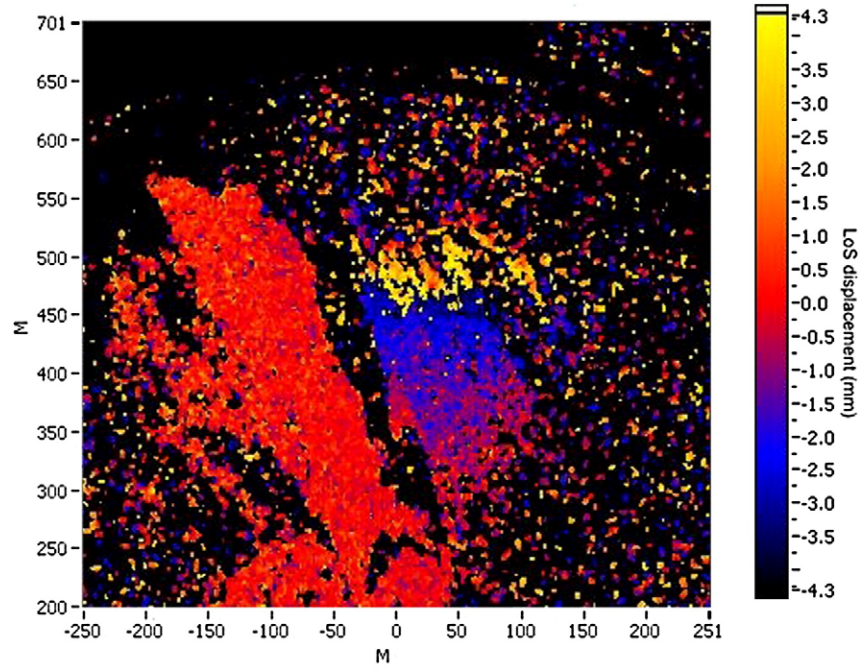

Fig. 11. Interferogram of the SdF between 14:30 UT and 14:41 UT of 27 February (time interval of 11 min), showing a deformation pattern related to landslide movements.

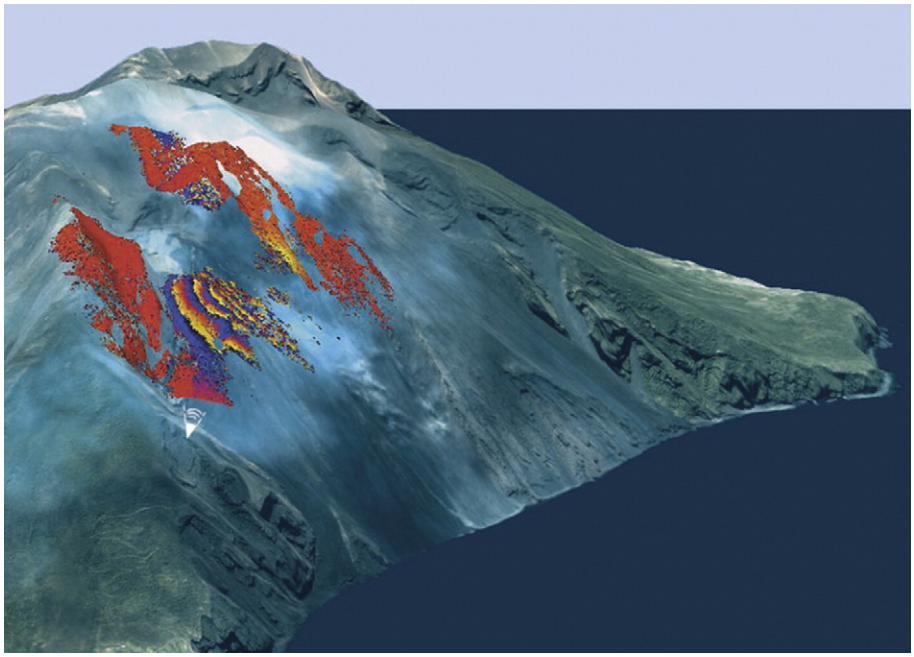

Fig. 12. 3D model of the Stromboli Island (Sciara del Fuoco slope and NE crater) with an interferogram obtained from the GB-InSAR. The position of the radar is shown with the white symbol. The interferogram with a time interval of 11 min (from 11:17 UT and 11:28 UT of 9 March 2007) shows a velocity greater than 300 mm/h.

the vent at 500 m a.s.l. and the explosion, showed a constant value of about 0.5 mm/h towards the sensor (Fig. 8). In the morning of 15 March a rapid increase in velocity was recorded in the crater sector (up to 7.00 mm/h). This deformation lasted until 20:37 UT on 15 March, when the explosion occurred.

Differently from most volcano InSAR studies, that are a snapshot and have finite strain results, the GB-InSAR installed at Stromboli allowed a continuous record, producing high-resolution signals of evolving patterns. For this reason, during the whole effusive phase (from 27 February to 12 April) the GB-InSAR was able to record, on the crateric area, two loops of deformation towards and backwards with respect to the sensor (shown respectively with red and blue lines in Fig. 8). These velocity inversions were observed by the radar for the first time in Stromboli since its installation in February 2003 (Casagli et al., 2003; Antonello et al., 2004b) and are related to inflation/deflation cycles. In details, the GB-InSAR recorded, on the crater area, an inflation before the opening of each effusive vent, and a deflation afterwards.

After 12 April (post-effusive phase), the eruption was considered to be completed and the velocity recorded by GB-InSAR progressively decreased down to values characteristic of the normal activity of the Stromboli volcano (Fig. 8).

5. Numerical modelling

5.1. Conceptual model

A stress–strain analysis of the Stromboli volcano was performed using the FLAC 3D code (Fast Lagrangian Analysis of Continua in 3 Dimensions) (ITASCA, 2005), a three-dimensional explicit finite difference numerical code for engineering and geomechanical simulations. This code permits the discretization of the geotechnical problem using a grid adjusted to fit the shape of the object to be modelled. Materials are represented by elements and each element behaves according to a prescribed linear or non linear stress/strain law, in response to the applied forces and boundary restraints. The code allowed the simulation of the effects of the intrusive dyke propagation or sheets of different geometries on the stability of the volcano flanks.

The simulation was implemented to investigate the stress–strain field associated to the presence of magma filling the magmatic conduit and to foresee the evolution of the magmatic feeding complex, identifying the most probable directions of propagation of new sheets and the effects of their propagation on the stability conditions of the volcano edifice.

The simulation was implemented in successive stages, overcoming the code inability to reproduce a continuous evolutionary process. The geometry and the magma pressure for each successive stage were defined assuming the results of the previous stages as conditions for the next one and verifying the evidences detected by in situ survey (Fig. 14).

The volcano edifice was discretized by a regular grid with cell size of 100 m. The sheets are represented as discontinuities of the grid and are modelled by means of interfaces. The magmatic pressure is imposed to the model as normal pressure applied on both sides of the interfaces. An elasto-plastic constitutive law was adopted and an homogeneous Mohr–Coulomb strength criterion was chosen for the volcanic cone, considering one lithotechnical unit (alternation of lava and breccia layers “lava-breccia unit”— Apuani et al., 2005a,b). No superficial incoherent materials are considered.

The groundwater conditions were imposed assuming the volcanic edifice saturated in the portion below the sea level, and dry above. This is consistent with the general absence of springs on the Stromboli Island. The material properties are summarized in Table 1.

The results of each simulation, expressed in terms of strain increments or displacements, represent the equilibrium state under the imposed new conditions.

Simplifications, necessarily imposed by numerical modelling procedure, allow results to be compared to the in situ observations,

Fig. 13. (A) Inverse of velocity vs. time diagram during the 8–9 March event. The decreasing linear trend allowed the forecast of the onset time for the new vent with an error of 30 min (predicted time: 9 March 2007 14:00 UT; observed: 9 March 2007 14:30 UT) — (B) Interferogram and its close up spanning a time interval of 11 min between 11:17 UT and 11:28 UT of 9 March 2007.

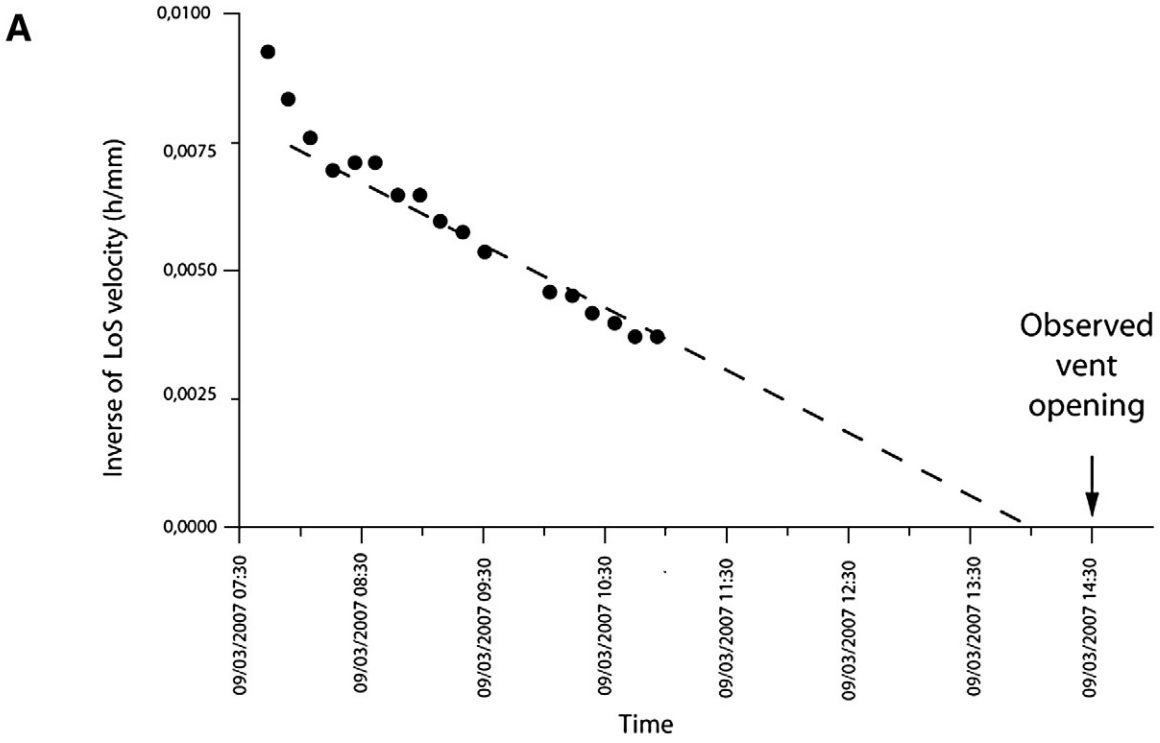
A
0,0100
0,0075
0,0050
0,0025
0,0000
Inverse of LoS velocity (h/mm)
Observed
vent
opening
09/03/2007 07:30
09/03/2007 08:30
09/03/2007 09:30
09/03/2007 10:30
09/03/2007 11:30
09/03/2007 12:30
09/03/2007 13:30
09/03/2007 14:30
Time

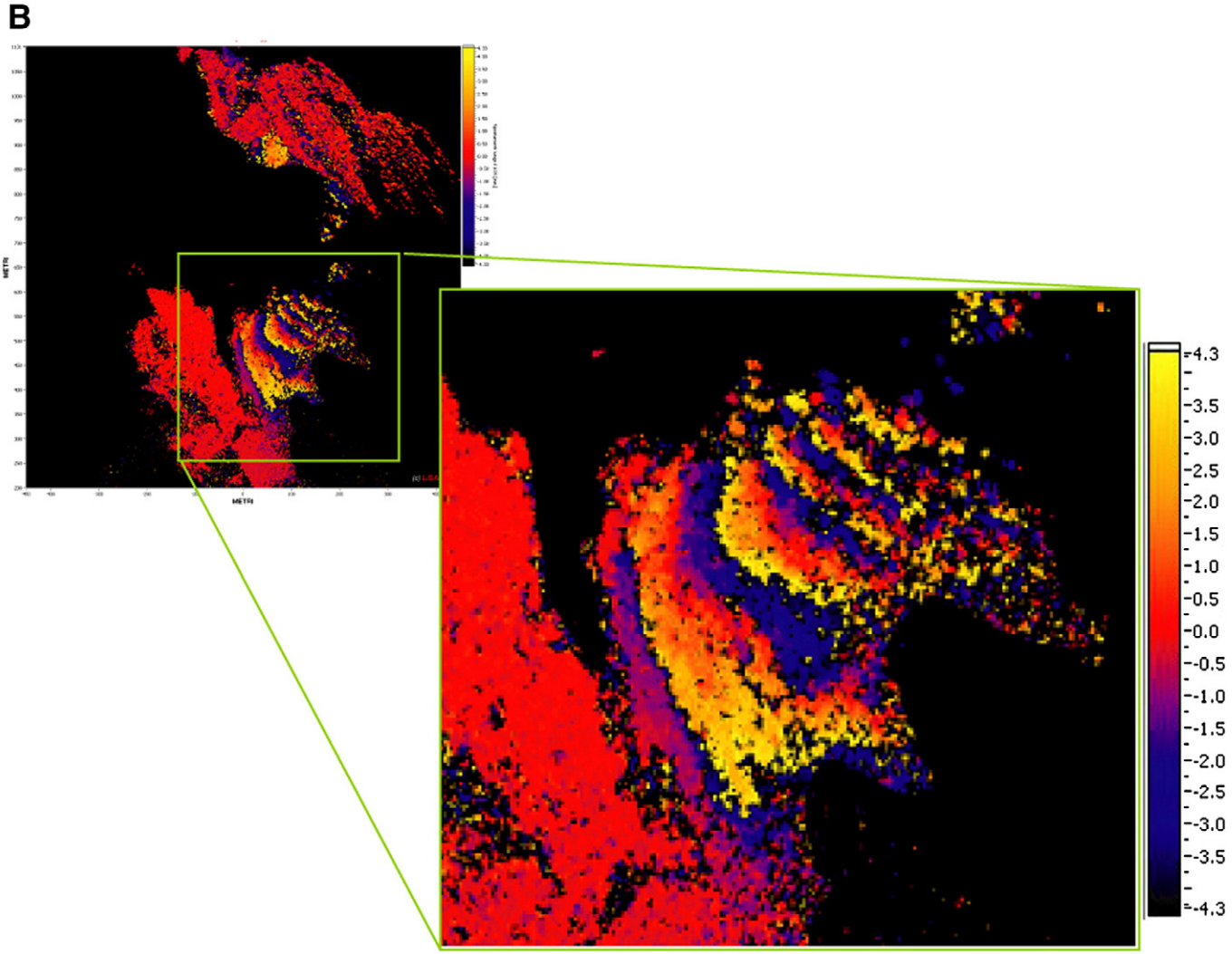
B
4.3
3.5
3.0
2.5
2.0
1.5
1.0
0.5
0.0
-0.5
-1.0
-1.5
-2.0
-2.5
-3.0
-3.5
-4.3

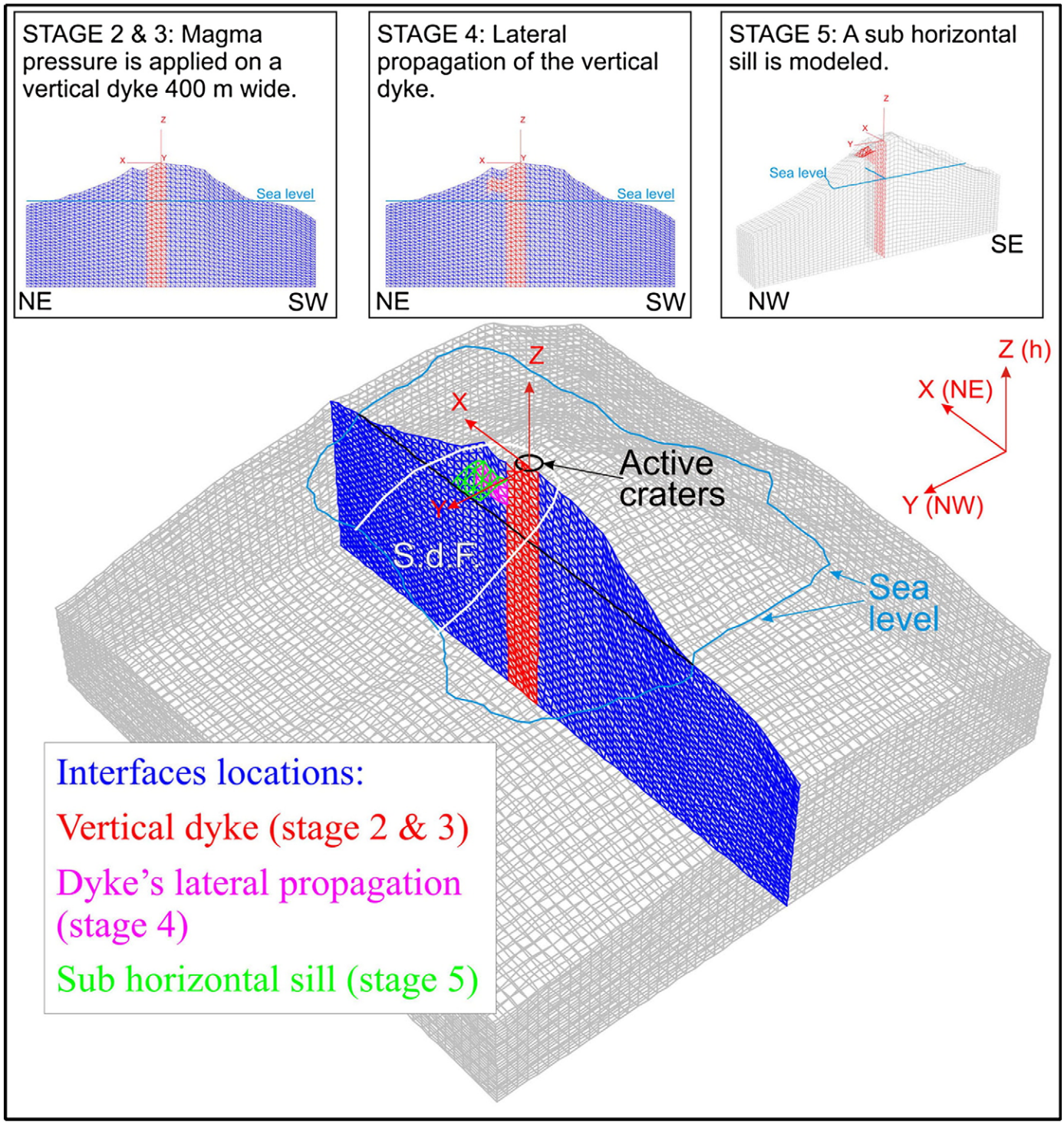

Fig. 14. Conceptual model: the Stromboli volcano (both sub aerial and submerged parts) is divided into a regular grid. The modelled area is 6 × 6 km, from the volcano top to − 1800 m b.s.l. The magma pressure is applied as a normal stress on the interfaces represented in red, magenta and green. Different stages were implemented to simulate different progressive conditions of the magmatic feeding system.

including the SAR interferometry record, in terms of distributions and trends rather than expecting equivalence in absolute values.

5.2. Procedure and results

The first step of the simulation was meant to achieve the state of initial equilibrium and to determine the stress configuration, due to the effect of the volcanic geometry. The stress field is a crucial factor in determining the intrusion directions of the sheets, generally developed along the σ_1–σ_2 plane, perpendicular to the least principal stress σ_3.

The second step was aimed at simulating the partial filling of the magmatic conduit, with magma level placed 50 m below the active craters. This condition represents the ordinary state for the Stromboli, characterized by a constant partial fill of the active dyke during the non paroxysmal activity with regular emission of gas and lava fountains. The active dyke was modelled as a vertical plane located below the active craters and striking SW–NE. Magma pressure was

Table 1
Material properties assigned to the volcanic cone lithotechnical unit.

Parameter	Symbol	Measure unit	Value
Elastic modulus	E	MPa	2.00E+09
Poisson ratio	ν		0.28
Friction	Φ	°	35
Cohesion	c	MPa	1
Tensile strength	T	Pa	1.10E+04
Dry unit weight	γ_d	kN/m^3	19
Saturated unit weight	γ_{sat}	kN/m^3	21

applied for a horizontal range of 400 m from the bottom of the edifice to the assumed magma raising level.

The paroxysmal eruption was simulated in stage three raising the magma level till the height of the main craters and applying a little amount of overpressure. This stage can represent the above-mentioned "pre-effusive phase" before the 2007 eruption. The applied amount of magma pressure incorporates both the magma-static component and the excess pressure acting as a driving force for the magmatic eruption. The magma-static pressure, linearly increasing with depth, was calculated as $P_m = \gamma h$, where γ is the magma unit weight, assumed equal to 25 kN/m^3 and h is the height of the magma column. A value of overpressure between 0 and 1 MPa was added to simulate the paroxysmal eruption.

The results of this stage, expressed in terms of deformations and concentration of the shear strain increments, show a maximum displacement of about 1 m. The most deformed region has an elliptical shape and is located in the upper part of the SdF, 200 m to the NW of the eruptive craters. The distribution of the shear strain increment evidences the presence of a highly disturbed portion in correspondence of the SdF flanks. (Fig. 15A). This horseshoe-shaped region is a weakened zone and can represent a preferential location for the intrusion of dyke swarm, in accordance with field structural data (Tibaldi, 2001, 2003). The superficial movements indicate local instability, which might evolve in shallow landslides if triggering factors progress, but are not sufficient to suggest the development of deep seated collapse of the volcano flanks, and the model always reaches the equilibrium condition (Fig. 15B).

The new stress field induced by the magma presence at the borders of the dyke suggests a lateral propagation of the dyke in the direction along which the tensile stresses are maximum (in absolute value), as shown by the resulting strain field in Fig. 16A. According to the normal stress distribution calculated in this stage, it is reasonable a lateral propagation of the dyke in the NE direction. This condition was implemented in the stage four of the analysis. In this stage the dyke is propagated by a lateral extrusion located at a depth of 200 m, and extended in the NE direction. The SW propagation, equally probable according to the model results, was

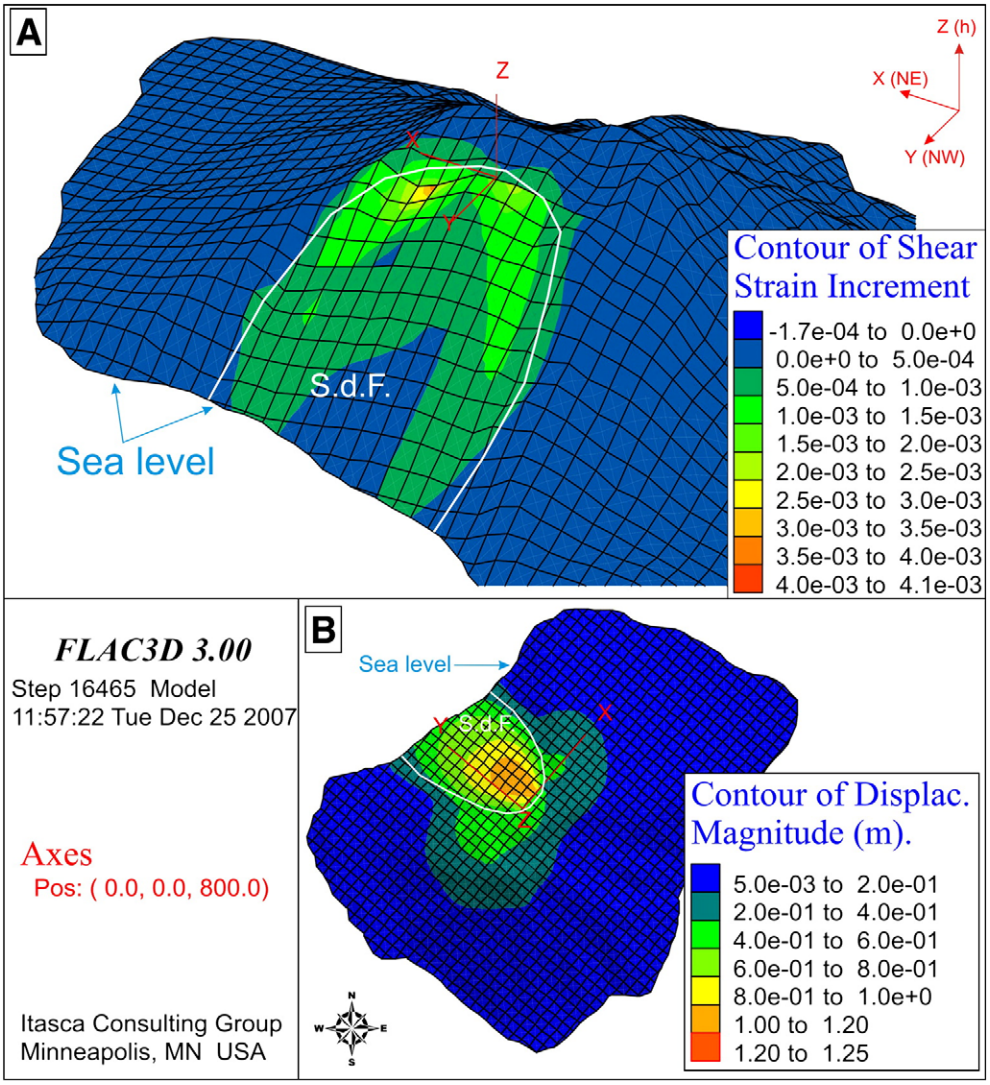

Fig. 15. Results of stage 3: (A) shear strain increment; (B) displacement contours. A deformation concentration along the Sciara del Fuoco depression is shown.

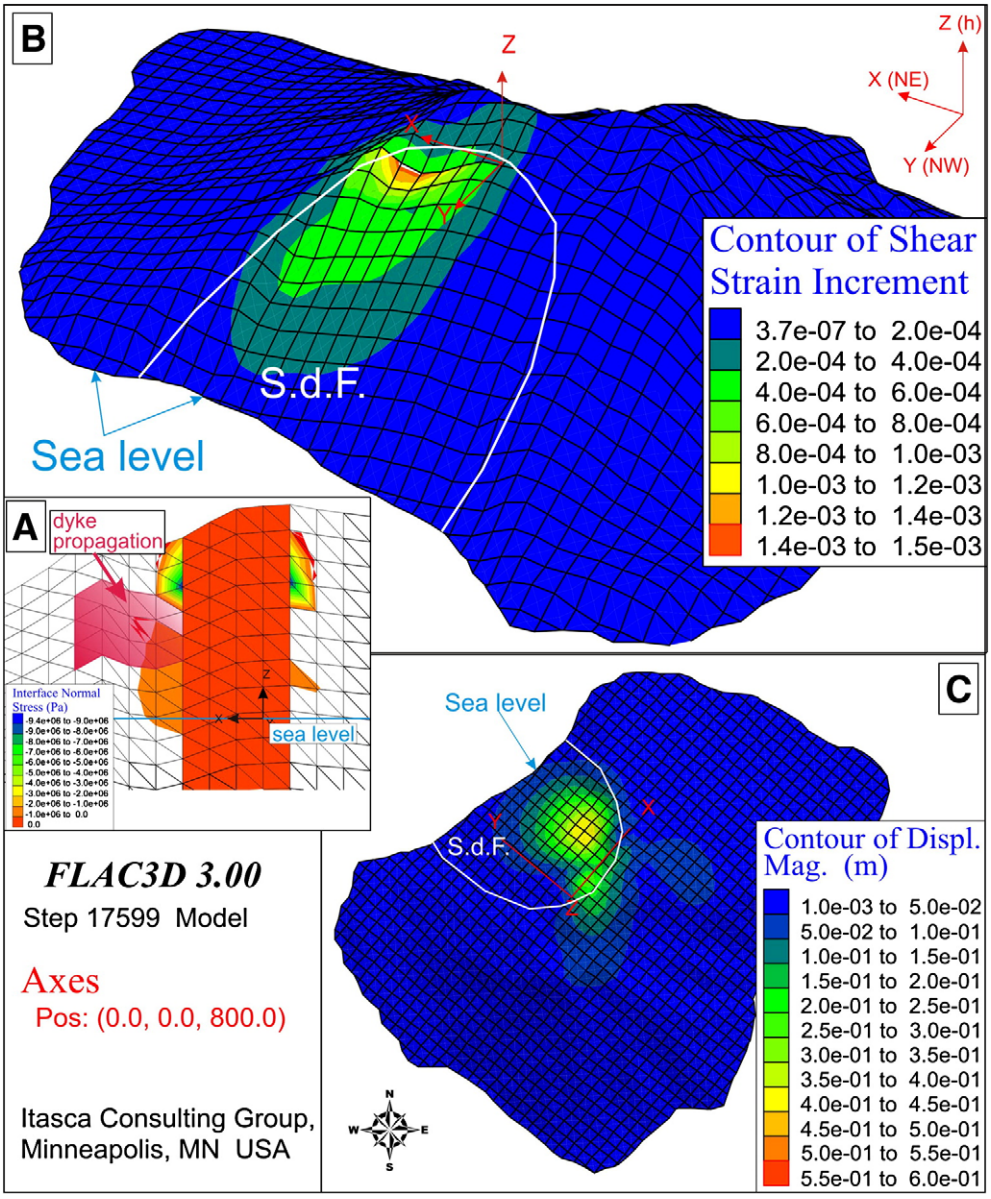

Fig. 16. Results of stage 4: (A) the dyke is propagated according to results of stage 3 in the direction in which the tensile stresses are higher (in absolute value). (B) and (C): shear strain increment and displacement contours show concentration on the NE sector of the Sciara del Fuoco.

rejected because no evidence of that was surveyed on site. The stress/strain analysis related to this phase shows displacements in the order of half a meter, with the most deformed zone located in the central part of the SdF (Fig. 16C). The shear strain increment contours indicate an upward propagation of the dyke and the development of local instability in the upper part of the SdF (Fig. 16B), in accordance with the tension cracks observed in the upper part of the SdF (Fig. 4).

The last stage (stage five) was aimed at modelling the possible mechanisms for explaining the formation of the eruptive vent on the SdF slope at about 500 m in altitude. Taking into account all the available data (field, interferometric, etc.) which indicate a wide area of bulging of the upper SdF at the foot of the northern summit crater during the 2007 eruption, the propagation of magma was modelled by a sub-horizontal sill intrusion starting from the NE–SW vertical dyke. As partial support of this hypothesis, the normal stress acting on a possible plane of sheet intrusion was analyzed and the results are compatible with the possibility of sill intrusion and propagation along the lower normal stress plane, as a result of stage four. A normal pressure was applied on the interface representing the sill in order to simulate the action exerted by the magma filling the sill. The effects of the magma pressure were analyzed. The resulting displacements are about 20 m and appear as a bulge of the SdF flank in the sector above the sill. The model does not reach equilibrium and deformation increases till the magma pressure is reduced. The model reaches the equilibrium conditions by introducing a pressure gradient that reduces the magma pressure to zero at the eruptive vent. This could be coherent with a mechanism of intrusion characterized by high magma pressure followed by its successive reduction when the magma reaches the surface and creates the vent. As the FLAC simulation cannot fully represent the propagation process, and since it is consequently impossible to define the transition from one condition to another, the induced deformation should be qualitatively considered in terms of extension and directions, rather than for its amount. The deformation modulus is, in this case, arbitrary and not significant. The shear strain increment contours indicate a highly stressed and disturbed band extended transversally to the SdF, at a height of about 550 m a.s.l. (Fig. 16). Furthermore, the maximum value of the shear strain increment is located in correspondence with the position of the eruptive vents. The proposed simulation seems to be

very coherent with the field evidence and it could represent the correct explanation for the observed 2007 phenomena.

6. Discussion

6.1. Intrusion of a NE–SW dyke

The integration of structural field observations, radar interferometry monitoring and numerical modelling provides complete information on the evolution of Stromboli volcano deformations during the 2007 eruption. The analysis of the entire dataset of GB-InSAR measurements, during the 2007 event, allowed the assessment of the deformation field of the monitored area. In details, the main deformation patterns recognized can be related to different factors:

1) the inflation/deflation respectively immediately before and after each new effusive event;
2) the bulging of localized sectors of the volcano involved in the vent opening;
3) the gravitational sliding of the SdF infill.

Changes in the deformation pattern are recorded by GB-InSAR in advance to each main event, therefore they can be considered as precursors.

The field observations carried out after 27 February 2007, suggest that the lava field created during that day and the conterminous area was affected by a swarm of dominant NE-striking fissures and dip-slip planes (Figs. 3–5). Their almost constant geometry and kinematics along strike are very important characteristics and indicate that they have been caused by a coherent stress/strain field. The strain and stress fields could be linked together in deformation scenarios induced by sub-volcanic intrusions (Muller and Pollard, 1977; Delaney and Pollard, 1982; Delaney et al., 1986; Pollard and Segall, 1987). When dykes approach the topographic surface, they are able to produce surface deformations as demonstrated by both numerical and field data, i.e. Gudmundsson and Loetveit (2005). These authors indicate that the main effects of a dyke propagating vertically upwards are, first, to close its boundary discontinuities/faults and then to encourage upward motions at both sides of the intruding dyke. Both an upward-directed magma force and a force acting normal to the dyke zone develop. These produce a topographic downward deflection above the dyke and a topographic upward deformation at the dyke sides. The resulting bulging of the topographic surface is elongated parallel to the dyke strike, as well as faulting and fracturing occur with the same parallel strike (Pollard, 1973; Gudmundsson and Loetveit, 2005). Dyke deflation produces a similar pattern, but with opposite motions. If these re-known criteria are applied to the deformation field observed during the 27 February 2007 events, it is possible to conclude that it could be the result of the intrusion of a NE-elongated sub-volcanic body.

The analysis of the stress distribution derived by the numerical simulation confirms the effects of the lateral propagation of the dyke in the NE direction (Fig. 16). The retrieved deformation pattern is consistent with the deformations recorded by GB-InSAR. Indeed, the computed strain field triggered by the intrusion of a dyke is localized on the upper part of the SdF sector and shows an analogous distribution to that observed by GB-InSAR monitoring on the NE upper sector of the SdF since 15 February.

The NE-striking dyke also produces a lateral magma force exerted on the dyke walls in a SE–NW direction, as previously suggested by a number of authors (Apuani et al., 2005a,b, 2007 and references therein). This lateral force can enhance the gravity instability of the SdF infill. The presence of possible recent wide deformations affecting the whole SdF infill is consistent with the structures found at the base of the summit pyroclastic cone (Fig. 6) and with the extensional fissures developed along the uppermost margin of the SdF depression, both S and N of the active crater zone. The summit cone is in fact offset by the swarm of steep NW-dipping slip planes, the attitude of which suggests they might be linked with deep-seated deformations.

6.2. Influence of the Stromboli structure on the NE–SW intrusions

The recent geological history of Stromboli, over the last 100 ky, has been characterized by a series of buildup phases of the edifice via dominant lava flows, interrupted by destruction phases of part of the cone, ranging from slow slope erosion to rapid removal of huge masses. Apart from one main flank collapse, which affected the SE part of the volcano in late Pleistocene times (Tibaldi, 1996, 2001), most sector and flank collapses occurred towards the NW, the youngest of which gave rise to the present SdF. This points out that the NW flank of the cone has been a zone of high slope instability throughout the last 13 ky.

The possible “draining” effect exerted by the debuttressed zone of the SdF depression on the magma rising into the cone was recently recognized (Tibaldi, 2004; Acocella and Tibaldi, 2005); this process in turn has the feedback effect of further enhancing slope instability. The Holocene geological history of the volcano indicates that when a sector collapse develops, sheet intrusions tend to expand preferentially along the shoulders of the amphitheatre depression or within it. These intrusions, can deform the infilling of the collapse depression thus producing smaller landslides capable, however, of triggering tsunamis.

The field structural data presented here indicates that before the 2007 events, a series of earlier deformations occurred in the SdF. The fissures appeared at the beginning of 2000 and widened in the following years, clearly show a deformation process affecting at least the S part of the SdF and unrelated to contemporaneous main magma intrusions. These fissures, striking NE–SW, were linked with the WNW–ESE left-lateral strike-slip plane, parallel to the southern flank of the last SdF lateral collapse. Some of the NE-striking fissures show a downthrow of the seaward block. These kinematics and the orientation and location of the various structures indicate that these acted as a whole under a coherent deformation field, consistent with seaward motions of the upper part of the southern SdF infill. Similar deformations probably acted also along the northern part of the SdF infill, suggesting that these earlier movements probably induced an extensional state of stress along the uppermost part of SdF, facilitating the upwelling of a huge amount of magma in the form of dykes. These dykes should have moved along NE–SW-striking planes following the normal direction to the local least principal stress (σ_3), as occurred during the 2002–2003 Stromboli crisis. This outcome is also consistent with the data presented on the very first phases of the development of the 2007 eruption. The data demonstrate that at the beginning (on 27 February), magma was emplaced through a NE-striking dyke across the northern part of the summit crater zone and propagated towards the NE.

The emplacement direction of the 2007 dyke is consistent, not only with the 2002–2003 event, but also with the recent geological–structural history of the volcano, when magma was mostly injected along the main NE-trending weakness zone, with single dykes striking from NNE to E–W (Tibaldi, 2003, 2004). In the Holocene, sheet intrusions into the NW cone flank were accompanied by frequent dyking also along the NE weakness zone, where single dykes and fissure eruptions had a dominant NE-strike and were concentrated in the zone between the summit crater and the present location of the Stromboli village. This suggests a shift of the magma paths NE, along the main weakness zone (Tibaldi et al., 2009; Corazzato et al., 2008).

6.3. From dyke to sill

The deformation pattern recorded by the GB-InSAR system in relation to the 9 March vent opening is quite different, so a different triggering mechanism must be considered. This is the reason why an

additional numerical simulation was made by considering a sub-horizontal sill intrusion to evaluate the resulting strain pattern. The idea of modelling a sill instead of a dyke is justified by the fact that field surveys at Stromboli revealed that the vertical dykes can abruptly bend into horizontal to sub-horizontal sills (Corazzato et al., 2008). This bending has been observed within a succession entirely made of scoria and breccia deposits, a lithology similar to the one that composes the SdF infill. Moreover, dyke feeding into sill is a widespread phenomenon observed in several volcanoes (i.e. Weertman, 1980; Corry, 1988; Gudmundsson, 1990; Gaffney et al., 2007; Pasquarè and Tibaldi, 2007; Tibaldi et al., 2008b). A sudden deviation from a dyke to a sill was also experimentally reproduced by Kavanagh et al. (2006), at the interface between an upper layer more rigid than a lower one. It has also been noted that magma paths can propagate by horizontal flow along sills showing finger-like lobes (Pollard et al., 1975). The main sill body may be a region that has coalesced into a sheet of magma, behind several propagating fingers. The fingers may be ancillary small intrusions, fed by the main body, rather than the distal propagating edge of a larger sheet intrusion (Pollard et al., 1975).

The interferometric fringes obtained from the GB-InSAR data of the 9 March events, are characterized by a semi-circular shape (Figs. 12 and 13). Considering the similarity between the deformation pattern derived from GB-InSAR monitoring and the strain pattern resulting from numerical simulation (Fig. 17), it is possible to hypothesize that the bulging immediately preceding the opening of the 9 March effusive vent might be related to the sub-horizontal sill intrusion. From this sill, fingers may have prolonged magma outwards from the main magma body up to the intersection with the SdF topographic surface and producing the new effusive vent.

An alternative interpretation is that the 9 March effusive vent has been produced by the intersection of a NW–SE-striking dyke with the SdF topographic surface. However, based on the available data, the interferometric fringes are not elongated in the NW–SE direction, which would suggest the presence of a NW–SE dyke. Such a hypothetic NW–SE dyke could not justify the wide bulge created in the previous deformation event.

Regarding the vent that opened on the afternoon 27 February at 400 m a.s.l., the GB-InSAR data and the field observations are not enough to constrain the intrusion mechanism; more direct observations of that area, during the local inflation phase preceding the vent opening, are necessary to assess if this vent was fed by a sill, by an inclined sheet, or by a dyke and with which orientation.

Summarizing, the validation of the interpretation of the available interferometric and field data via numerical modeling suggests that the 2007 effusion might have resulted from two different triggering

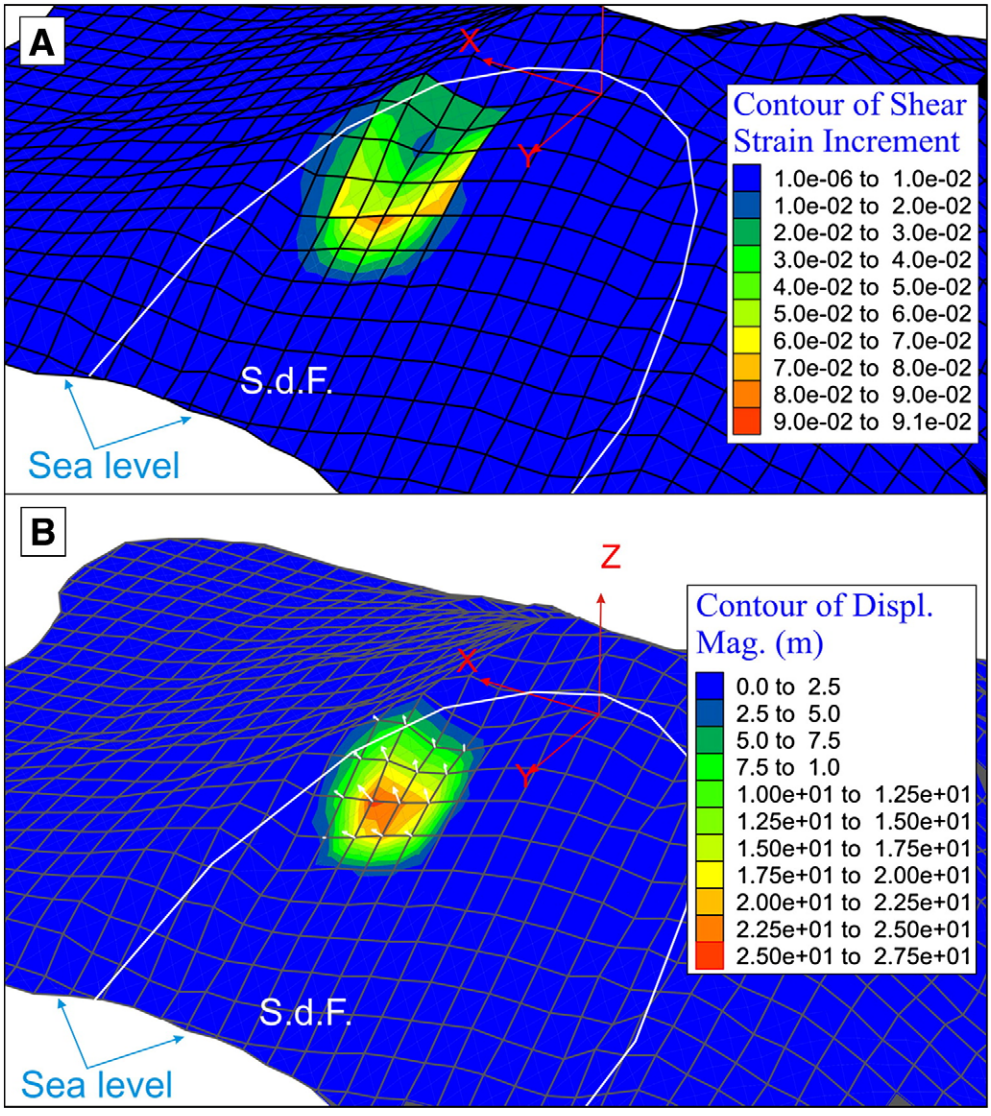

Fig. 17. Results of stage 5: A sub horizontal sill is introduced. (A): Contour of shear strain increment. (B): Displacement contours and displacement vectors (white arrows).

mechanisms: (1) the NE–SW dyke intrusion generating the inflation/deflation of the volcanic apparatus, and (2) the sub-horizontal sill intrusion producing the bulging of the area between the N active crater and the 9 March effusive vent.

7. Conclusions

The strain field developed during the 2007 events at Stromboli volcano is strictly related to the temporal evolution of the effusive activity. From the different types of data presented in this paper, it is possible to draw the following main conclusions:

1. field structural surveys show the presence of new fractures, mostly striking NE–SW, on the upper part of the SdF sector. These fractures are compatible with the intrusion of a NE–striking dyke;
2. GB-InSAR monitoring highlights different deformation patterns, related to the imminent eruption and to the new vent openings, suggesting different triggering mechanisms. Furthermore, the GB-InSAR system has recorded changes in the deformation patterns, both on the crater area and on the SdF sector, in advance to the onset of each of the relevant events;
3. strain field evaluated from numerical modelling confirms the hypothesis of two different types of intrusion that triggered different deformation patterns:

a. lateral propagation of the dyke in the NE direction (starting the 27 February eruption);
b. sub-horizontal sill intrusion starting from a dyke and producing the vent on 9 March.

The proposed integrated approach, based on a structural geological survey, interferometric radar monitoring and numerical modelling, represents a useful tool to bypass the limitations of the individual methodologies. Indeed, the structural geological survey allows the recognition of the surface deformation and the identification of the responsible stress field, but it is unable to provide continuous quantitative information. This limit is overcome by the ground-based radar, which provides a continuous monitoring of the deformation pattern especially in terms of its spatial and temporal evolution. However, it is unable to identify the triggering mechanism of deformation. Numerical simulations instead give useful information about the triggering mechanisms but they are unable to fully represent the propagation process and to define the transition from one condition to another. The deformation pattern retrieved from the numerical simulation should be considered just in terms of the extension of the deformed zone and in terms of directions of the deformation.

Acknowledgements

We would like to acknowledge the helpful comments of G. Wadge (Environmental System Science Centre, University of Reading) and an anonymous reviewer. This study was funded by the Italian Department of Civil Protection (DPC) through the Istituto Nazionale di Geofisica e Vulcanologia and DPC Stromboli emergency Project V2. This activity was performed in the framework of ILP-Task Force II, Project “New tectonic causes of volcano failure and possible premonitory signals” (Leader A. Tibaldi). The GB-InSAR system on the Stromboli volcano was set up on behalf of DPC. Prof. B. De Bernardinis and its group at the Department of Civil Protection are acknowledged for the support to the project and for the permission given for publication. The GB-InSAR data and the sensors employed in the monitoring of Stromboli volcano have been designed, produced and deployed by Ellegi-LisaLab s.r.l., on the technology licensed by the Joint Research Centre of Ispra-European Commission. The authors especially wish to thank D. Leva and C. Rivolta of Ellegi-LiSALab s.r.l., Dr. ML Ibsen of Kingston University is acknowledged for the language revision.

References

Acocella, V., Tibaldi, A., 2005. Dike propagation driven by volcano collapse: A general model tested at Stromboli, Italy. Geophysical Research Letters 32, L08308. doi:10.1029/2004GL022248.

Antonello, G., Casagli, N., Farina, P., Guerri, L., Leva, D., Nico, G., Tarchi, D., 2003. SAR interferometry monitoring of landslides on the Stromboli Volcano. Proceedings of FRINGE 2003 Workshop, 1–5 December 2003, ESA/ESRIN, Frascati, Italy.

Antonello, G., Casagli, N., Farina, P., Leva, D., Nico, G., Sieber, A.J., Tarchi, D., 2004a. Ground-based SAR interferometry for monitoring mass movements. Landslides 1, 21–28.

Antonello, G., Tarchi, D., Casagli, N., Farina, P., Guerri, L., Leva, D., 2004b. SAR interferometry from satellite and ground-based system for monitoring deformations on the Stromboli volcano. Proceedings IGARSS 2004 — International Geoscience and Remote Sensing Symposium, Anchorage, Alaska (USA).

Antonello, G., Casagli, N., Catani, F., Farina, P., Fortuny-Guasch, J., Guerri, L., Leva, D., Tarchi, D., 2007. Real-time monitoring of slope instability during the 2007 Stromboli eruption through SAR interferometry. Proceeding of 1st NACL, Veil (Colorado).

Apuani, T., Corazzato, C., Cancelli, A., Tibaldi, A., 2005a. Physical and mechanical properties of rock masses at Stromboli: a dataset for flank instability evaluation. Bulletin of Engineering Geology and the Environment 64 (4), 419–432.

Apuani, T., Corazzato, C., Cancelli, A., Tibaldi, A., 2005b. Stability of a collapsing volcano (Stromboli–Italy): limit equilibrium analysis and numerical modelling. In: Gudmundsson, A., Acocella, V. (Eds.), The Tectonics and physics of volcanoes. Special issue, Journal of Volcanology and Geothermal Research, vol. 144(1–4), pp. 191–210.

Apuani, T., Merri, A., Masetti, M., 2007. Effects of volcanic seismic events on the Stromboli stability by finite difference numerical modeling. In: Volcanic Rocks — Malheiro & Nunes (Eds): Proceedings of the international workshop on volcanic rocks, workshop W2 — 11th Congress ISRM Ponta Delgada, Azores, Portugal, July, 14–15 2007.

Atzeni, C., Canuti, P., Casagli, N., Leva, D., Luzi, G., Moretti, S., Pieraccini, M., Sieber, A., Tarchi, D., 2001. Monitoring unstable cultural heritage sites with radar interferometry. In: Sassa, K. (Ed.), 'UNESCO/IGCP Symposium on Landslide Risk Mitigation and Protection of Cultural and Natural Heritage'. Tokyo, Japan, 15–19 January 2001, pp. 257–264.

Calvari, S., Lodato, L., Harris, A.J.L., Cristaldi, A., Steffke, A., Spampinato, L., 2009-submitted for publication. The 2007 Stromboli flank eruption: chronology of the events from images recorded by the INGV web-cameras network and from daily helicopter surveys, and effusion rate measurements from thermal images and satellite data. J. Volcanol. Geotherm. Res.

Casagli, N., Farina, P., Guerri, L., Tarchi, D., Fortuny, J., Leva, D., Nico, G., 2003. Preliminary results of SAR monitoring of the Sciara del Fuoco on the Stromboli volcano. Occurrence and Mechanisms of Flow-like Landslides in Natural Slopes and Earthfills, Sorrento, Italy, Patron Editore, Bologna.

Casagli, N., Farina, P., Leva, D., Tarchi, D., 2004. Landslide monitoring on the Stromboli volcano through SAR interferometry. Proceedings of 9th International Symposium on Landslides, Rio de Janeiro, Brasil.

Chevallier, L., Verwoerd, W.J., 1988. A numerical model for the mechanical behaviour of intraplate volcanoes. Journal of Geophysical Research 93 (B5), 4182–4198.

Chouet, B., Dawson, P., Ohminato, T., Martini, M., Saccorotti, G., Giudicepietro, F., De Luca, G., Milana, G., Scarpa, R., 2003. Source mechanism of explosions at Stromboli volcano, Italy, determined from moment tensor inversions of very-long-period data. Journal of Geophysical Research 108 (B1). doi:10.1029/2002JB001919.

Corazzato, C., 2005. A Quantitative study of volcano lateral collapses: the example of Stromboli (Italy). PHd Thesis. Tutors: Tibaldi, A. & Apuani, T. Unpubl.

Corazzato, C., Francalanci, L., Menna, M., Petrone, C.M., Renzulli, A., Ribaldi, A., Vezzoli, L., 2008. What controls sheet intrusion in volcanoes? Structure and petrology of the Strombol sheet complex, Italy. Journal of Volcanology and Geothermal Research 173, 26–54. doi:10.1016/j.jvolgeores.2008.01.006.

Corry, C.E., 1988. Laccoliths—Mechanics of emplacement and growth. Geological Society of America, Special Paper, vol. 220. 110 pp.

Curlander, J.C., McDonough, R.N., 1991. Synthetic Aperture Radar: Systems and Signal Processing. John Wiley and Sons, New York. 672 pp.

Delaney, P.T., Pollard, D.R., 1982. Solidification of basaltic magma during flow in a dike. American Journal of Science 282, 856–885.

Delaney, P.T., Pollard, D.D., Ziony, J.I., McKee, E.H., 1986. Field relations between dykes and joints: emplacement processes and paleostress analysis. Journal of Geophysical Research 91, 4920–4938.

Ferrari, L., Garduño, V.H., Neri, M., 1993. I dicchi della Valle del Bove, Etna: un metodo per stimare la dilatazione degli apparati vulcanici. Memorie Società Geologica Italiana 47, 495–508.

Fukuzono, T., 1985a. A new method for predicting the failure time of a slope failure. Proc. 4th Int. Conf. and Field Workshop on Landslides, Tokyo (Japan), pp. 145–150.

Fukuzono, T., 1985b. A method to predict the time of slope failure caused by rainfall using the inverse number of velocity of surface displacement. Journal Japanese Landslide Society 22, 8–13.

Fukuzono, T., 1990. Recent studies on time prediction of slope failure. Landslide News 4, 9–12.

Gabbianelli, G., Romagnoli, C., Rossi, P.L., Calanchi, N., 1993. Marine geology of the Panarea–Stromboli area (Aeolian Archipelago, Southeastern Tyrrhenian sea). Acta Vulcanologica 3, 11–20.

Gaffney, E.S., Damjanac, B., Valentine, G.A., 2007. Localization of volcanic activity: 2. Effects of pre-existing structure. Earth and Planetary Science Letters 263, 323–338.

Gillot, P.Y., Keller, J., 1993. Radiochronological dating of Stromboli. Acta Vulcanologica 3, 11–20.

Gudmundsson, A., 1990. Emplacement of dikes, sills and crustal magma chambers at divergent plate boundaries. Tectonophysics 176, 257–275.

Gudmundsson, A., Loetveit, I.F., 2005. Dyke emplacement in a layered and faulted rift zone. Journal of Volcanology and Geothermal Research 144, 311–327.
ITASCA, 2005. FLAC3D (Fast Lagrangian Analysis of Continua in 3 Dimensions). User's guide. ITASCA Consulting Group, Minneapolis, MN.
Kavanagh, J.L., Menand, T., Sparks, R.S.J., 2006. An experimental investigation of sill formation and propagation in elastic media. Earth Planetary Science Letters 245, 799–813.
Keller, J., Hornig-Kjarsgaard, I., Koberski, U., Stadlbauer, E., Francalanci, L., Lenhart, R., 1993. Geology, stratigraphy, and volcanological evolution of the island of Stromboli, Aeolian Arc, Italy. Acta Vulcanologica 3, 21–68.
Manetti, P., Pasquarè, G., Tibaldi, A., Tsegaye, A., 1989. Geologia dell'Isola di Alicudi (Arcipelago delle Eolie). Bollettino Gruppo Nazionale Vulcanologia 2, 903–916.
Muller, O.H., Pollard, D.D., 1977. The stress state near Spanish peaks, Colorado, determined from a dike pattern. Pure and Applied Geophysics 115, 69–86.
Pasquarè, F., Tibaldi, A., 2007. Structure of a cone sheet swarm unraveling the interplay between tectonic and magma stresses at Mt. Esja, SW Iceland. Journal of Volcanology and Geothermal Research 161, 131–150.
Pasquarè, G., Francalanci, L., Garduno, V.H., Tibaldi, A., 1993. Structure and geological evolution of the Stromboli volcano, Aeolian islands, Italy. Acta Volcanologica 3, 79–89.
Pollard, D.D., 1973. Derivation and evaluation of a mechanical model for sheet intrusions. Tectonophysics 19, 233–269.
Pollard, D.D., Segall, P., 1987. Theoretical displacement and stresses near fractures in rock: with applications to faults, joints, veins, dikes, and solution surfaces. In: Atkinson, B.K. (Ed.), Fracture Mechanics of Rock. Academic Press, Inc., pp. 277–349.
Pollard, D.D., Muller, O.H., Dockstader, D.R., 1975. The form and growth of fingered sheet intrusions. Geological Society of America Bulletin 3, 351–363.
Romagnoli, C., Kokelaar, P., Rossi, P.L., Sodi, A., 1993. The submarine extension of Sciara del Fuoco feature (Stromboli Is.): morphological characterization. Acta Volcanologica 3, 91–98.
Rudolf, H., Tarchi, D., 1999. LISA: The Linear SAR Instrument. DG JRC, European Commission, Technical Note No. I.99.126. July 1999.
Rudolf, H., Leva, D., Tarchi, D., Sieber, A.J., 1999. A mobile and versatile SAR system. Proceedings of IGARSS 1999, Hamburg, Germany, 28 June–2 July, pp. 592–594. doi:10.1109/IGARSS.1999.773575.
Sachpazi, M., Kontoes, Ch., Voulgaris, N., Laigle, M., Vougioukalakis, G., Sikioti, Olga, Stavrakakis, G., Baskoutas, J., Kalogeras, J., Lepine, J.Cl., 2002. Seismological and SAR signature of unrest at Nisyros caldera, Greece. Journal of Volcanology and Geothermal Research 116, 19–33.
Tarchi, D., Ohlmer, H., Sieber, A.J., 1997. Monitoring of structural changes by radar interferometry. Research in Nondestructive Evaluation 9, 213–225.
Tarchi, D., Rudolf, H., Pieraccini, M., Atzeni, C., 2000. Remote monitoring of buildings using a ground-based SAR. International Journal of Remote Sensing 21 (18), 3545–3551.
Tarchi, D., Casagli, N., Fanti, R., Leva, D., Luzi, G., Pasuto, A., Pieraccini, M., Silvano, S., 2003. Landslide monitoring by using ground-based SAR interferometry: an example of application to the Tessina landslide in Italy. Engineering Geology 68, 15–30.
Tibaldi, A., 1996. Mutual influence of diking and collapses at Stromboli volcano, Aeolian Arc, Italy. Geol. Soc. Spec. Publ., London, vol. 110, pp. 55–63.
Tibaldi, A., 2001. Multiple sector collapses at Stromboli volcano, Italy: how they work. Bulletin of Volcanology 63 (2/3), 112–125.
Tibaldi, A., 2003. Influence of volcanic cone morphology on dikes, Stromboli, Italy. Journal of Volcanology and Geothermal Research 126, 79–95.
Tibaldi, A., 2004. Major changes in volcano behavior after a sector collapse: insights from Stromboli, Italy. Terra Nova 16, 2–8. doi:10.1046/j.1365-3121.2003.00517.x.
Tibaldi, A., in press. A new geological map of Stromboli volcano (Tyrrhenian Sea, Italy) based on application of lithostratigraphic and UBS units. Geological Society of America, Special Publication.
Tibaldi, A., Pasquarè, G., Francalanci, L., Garduno, V.H., 1994. Collapse type and recurrence at Stromboli volcano, associated volcanic activity, and sea level changes. Accademia dei Lincei, Atti dei Convegni Lincei, Roma 112, 143–151.
Tibaldi, A., Corazzato, C., Apuani, T., Cancelli, A., 2003. Deformation at Stromboli volcano (Italy) revealed by rock mechanics and structural geology. Tectonophysics 361, 187–204.
Tibaldi, A., Apuani, T., Corazzato, C., Pasquaré, F.A., Vezzoli, L., 2009. Geological–structural framework of Stromboli Volcano, past collapses, and the possible influence on the events of the 2002–03 crisis. AGU Monographs n. 182.
Tibaldi, A., Corazzato, C., Kozhurin, A., Lagmay, A.F.M., Pasquaré, F.A., Ponomareva, V., Rust, D., Tormey, D., Vezzoli, L., 2008a. Influence of substrate tectonic heritage on the evolution of volcanoes: predicting sites of flank eruptions, lateral collapses, and erosion. Global Planetary Change 61, 151–174. doi:10.1016/j.gloplacha.2007.08.014.
Tibaldi, A., Vezzoli, L., Pasquaré, F.A., Rust, D., 2008b. Strike-slip fault tectonics and the emplacement of sheet–laccolith systems: the Thverfell case study (SW Iceland). Journal of Structural Geology 30, 274–290.
Voight, B., 1988. Material science law applies to time forecast of slope failure. Landslide News 3, 8–11.
Voight, B., 1989. A relation to describe rate-dependent material failure. Science 243 (10), 125–130.
Voight, B., 2000. Structural stability of andesite volcanoes and lava domes. Philosophical Transactions of the Royal Society of London 358, 1663–1703.
Voight, B., Elsworth, D., 1997. Failure of volcano slopes. Geotechnique 47 (1), 1–31.
Weertman, J., 1980. The stopping of a rising, liquid-filled crack in the earth's crust by a freely slipping horizontal joint. Journal of Geophysical Research 85 (B2), 967–976.